Review

Recent Advancements in Doped/Co-Doped Carbon Quantum Dots for Multi-Potential Applications

Ganeshlenin Kandasamy [ORCID]

Department of Biomedical Engineering, St. Peter's Institute of Higher Education and Research, Chennai 600054, India; lenin.ganeshk@gmail.com

check for updates

Abstract: Carbon quantum dots (CQDs)/carbon nanodots are a new class of fluorescent carbon nanomaterials having an approximate size in the range of 2–10 nm. The majority of the reported review articles have discussed about the development of the CQDs (via simple and cost-effective synthesis methods) for use in bio-imaging and chemical-/biological-sensing applications. However, there is a severe lack of consolidated studies on the recently developed CQDs (especially doped/co-doped) that are utilized in different areas of application. Hence, in this review, we have extensively discussed about the recent development in doped and co-doped CQDs (using elements/heteroatoms—e.g., boron (B), fluorine (F), nitrogen (N), sulphur (S), and phosphorous (P)), along with their synthesis method, reaction conditions, and/or quantum yield (QY), and their emerging multi-potential applications including electrical/electronics (such as light emitting diode (LED) and solar cells), fluorescent ink for anti-counterfeiting, optical sensors (for detection of metal ions, drugs, and pesticides/fungicides), gene delivery, and temperature probing.

1. Introduction

Carbon quantum dots (CQDs) are a new class of fluorescent carbon nanomaterials having a size in the range of ~2–10 nm and are also known by different names including carbogenic nanoparticles, carbon nanoparticles (CNPs), carbon dots (CDs), or carbon nanodots (CNDs). Fluorescent CQDs were accidentally discovered in 2004 by Xu et al. while purifying single-walled carbon nanotubes derived from the arc-discharge soot [1]. Shortly after, Sun et al. prepared similar CQDs—with improved photoluminescence—in both solution/liquid and solid states (without any photo-bleaching/blinking effects) by adopting a simple surface passivation method (using molecules such as polyethylene glycol (PEG) and poly(propionylethyleneimine-co-ethyleneimine)), where the presence of energy traps on the surface of those CQDs have made them more emissive upon stabilization via passivation [2]. Later on, Cao et al. have explored the utilization of the surface-passivated CQDs in multi-photon bio-imaging by internalizing them inside the human breast cancer MCF-7 cells, where these CQDs have proved their capability to label both cell membrane and cytoplasm of the cancer cells [3]. Furthermore, in 2009, Yang et al. synthesized and consequently employed the surface-passivated CQDs in in vivo mice model imaging [4]. Thereafter, numerous research works have been carried out to effectively synthesize CQDs for different applications.

Initially, CQDs are prepared via laser ablation of a carbon target in the presence of water vapor, and then they are cost-effectively made via candle soot—collected by keeping a glass plate on top of smoldering candles [5]. Later, one-step/-pot thermal carbonization/oxidation based pyrolysis

method is introduced to synthesize the CQDs with either hydrophilic or organophilic surface characteristics, while using different citrate salts as the carbon sources [6,7]. Besides the above, methods such as silica spheres as carriers-based [8], carbon/natural gas/combustion soot-derived [9,10], microwave [11], pyrolysis [12], carbonization of precursors in non-coordinating solvents [13], hydrothermal [14,15], electrochemical [16], sonochemical [17], stöber [18], bio(fruit/leaf) extraction [19], thermal carbonization/decomposition [20], and polyol [21] are the other common synthesis methods used in the effective preparation of the CQDs. Baker et al. [22] and Silva et al. [23] have majorly reviewed about (i) these synthesis methods that were developed during the time period of 2004–2011 to prepare CQDs, and (ii) the corresponding physicochemical properties—including crystalline nature, hybridization, single-photon or multi-photon excitation (such as near-ultraviolet (near-UV), UV, infrared (IR) and/or near-IR wavelengths), and optical properties (such as absorbance, photoluminescence, photo-induced electron transfer and redox properties, and electrochemical luminescence). Based on their review, it can be observed that most of the research workup to2011 has solely focused on the in vitro/in vivo bio-imaging application of the CQDs.

However after 2011, the CQDs are prepared—with/without doping and/or surface passivation/functionalization [24–26]—for wide range of applications including white light-emitting devices (WLEDs) [27], sensors for small chemical molecules (such as phosphates, glucose, and α-fetoprotein)/metal ions, and biological molecules (e.g., protein and deoxyribo-/ribo-nucleic acids (DNA/RNA)) [28–36], electroluminescence luminophore [37], self-cleaning infrared nano-sensors [38], fluorescent inks for printing luminescent patterns (useful in anti-counterfeit and optoelectronics/photoelectronics) [39–42], energy devices [43], photocatalysts and electrocatalysts [44], drug delivery [45,46], cancer therapy [47], and so on. Nevertheless, the majority of the reported review articles after 2011 have majorly discussed the development of CQDs (via simple and cost-effective synthesis methods) for use in bio-imaging and chemical-/biological-sensing applications. Hence, there is a severe lack of consolidated studies on the recently developed CQDs (especially doped/co-doped) that are utilized in different areas of application. Thus, in this review, we have systematically discussed the recent developments in the synthesis of the doped and co-doped CQDs, and also about their emerging multi-potential applications, including electrical/electronics (such as LED and solar cells), fluorescent ink for anti-counterfeiting, optical sensors (for detection of metal ions, drugs, and pesticides/fungicides), gene delivery, and temperature probing.

2. Carbon Quantum Dots (CQDs)

2.1. Un-Doped CQDs

Un-doped CQDs are the normal CQDs possessing carbon atoms with sp^2 & sp^3 configurations at altering proportions [26], and also a general composition of hydrogen (H) and oxygen (O), apart from the major carbon (C) atoms. Usually, these un-doped CQDs are made by using a variety of naturally available and/or synthetic molecular precursors as carbon sources along with/without surface-passivation via different synthesis methods (mentioned as above), where surface passivation is the formation of a thin layer of insulation surrounding the CQDs—implemented to improve their optical properties by diminishing the negative effects of the surface contamination. The commonly used carbon sources are given as follows: fruit and vegetable extracts (extracts from saccharum officinarum, lemon, banana, strawberry, grape, orange (pericarp/waste peels), papaya, pomelo peel, cabbage, watermelon peel, sweet potato, sweet red pepper, rose heart radish, tulsi leaves, lotus root, soy milk, and willow bark), grass, aloe, pseudo-stem of banana plant, rice flour, cashew gum, silk, barbecue meat, chicken eggs, honey, almonds, coconut water, resins, hair fibres, ascorbic acid, PEG, arginic acid, arginine, cysteine, animal skins, bovine serum albumin, citric acid, glucosamine, glycerol, glutaraldehyde, carbohydrates, saccharides, maltose, starch, sucrose, dextran, and ortho-/para-/meta-phenylenediamine [48–50]. Moreover, the following are the generally utilized surface passivating agents: PEG, urea, thio-urea, histidine, β-alanine, ethylene

diamine, 1-hexadecylamine, poly(propionylethyleneimine-co-ethyleneimine), poly(ethyleninmine), tris-(hydroxymethyl) aminomethane, 4,7,10-trioxa-1,13-tridecanediamine, 4-arm amine-terminated ribonuclease, poly(ethylenimide)-b-PEG-b-poly(ethylenimide), tetraoctylammonium bromide, polyvinyl pyrrolidone (PVP), 6-aminocaproic acid, and dipotassium hydrogen phosphate [24,46,51–54].

2.2. Doped CQDs

Doped CQDs are commonly prepared via doping of the hetero-atoms—e.g., boron (B), fluorine (F), nitrogen (N), sulphur (S), and phosphorous (P)—into the general composition (i.e., C, H and O) of the CQDs (to yield B-/F-/N-/P- and S-doped CQDs, respectively) [55,56]. In addition, co-doping of these (B, F, N, P, and/or S) heteroatoms into the CQDs is also performed [25,57]. Generally, doping and/or co-doping are mainly performed to control the photoluminescence phenomenon in the CQDs for improving their fluorescence efficacy, which is measured in terms of quantum yield (QY%) [58–60].

2.2.1. B-Doped CQDs

Shan et al. (2014) initially fabricated the B-doped CQDs—with blue emission and QY of 14.8%—via solvothermal method (2 h at 200 °C) by using boron tribromide (BBr_3, as B dopant), and hydroquinone (as C precursor) [61]. Then, Bourlinos et al. (2015) have synthesized olive-green colored B-doped CQDs by microwave heating (700 W for 4 min) of an aqueous solution of citric acid, boric acid (as B dopant) and urea, where the excitation of the CQDs at 350 nm has given an emission band at 450 nm corresponding to blue photoluminescence with QY of 10–15% [62]. Moreover, B doping in the CQDs has caused a significant improvement in the non-linear optical response in comparison to the un-doped CQDs. In a similar study, Jana et al. (2017) have used modified hydrothermal treatment (7 h at 200 °C) to prepare different kinds of B doped CQDs (with QYs in the range of 2.1–5.4%) by utilizing a mixture of ascorbic acid (as C source) and various B precursors including boric acid, sodium borohydride, sodium borate, and borax [63]. Moreover, in another recent study, Jia et al. (2019) have prepared B doped CQDs via hydrothermal method (10 h at 200 °C) by utilizing phenylboronic acid as the precursor material (self-doping—i.e., as both C source and B dopant), where these CQDs have possessed excitation/emission wavelength of 247/323 nm, and improved QY of 12% [64].

2.2.2. F-Doped CQDs

Zuo et al. (2017) prepared F-doped CQDs via solvothermal method (8 h at 180 °C) by using citric acid as the C source, and 4,5-difluorobenzene-1,2-diamine as the F source (due to the high stability of F atom in aromatic ring), and compared them with un-doped CQDs—prepared by using o-phenylenediamine as the carbon sources, as shown in Figure 1 [65]. F-doped CQDs have displayed (i) yellow light emission under the excitation wavelength of 480 nm, and (ii) higher QYs of 31% and 14% at the corresponding emission wavelengths of 550 nm and 600 nm, in comparison to the QYs of 28% and 11% for un-doped CQDs at emission wavelengths of 500 and 550 nm, respectively. In a further study, the same authors (Zuo et al., 2018) have prepared F-doped cationic CQDs through solvothermal process (6 h at 180° C) by using tetrafluoroterephthalic acid (TFTA) as F source, and 1.8K branched polyethyleneimine (1.8K b-PEI) as +ve charge site source. F-CQDs have shown a nuclear/polymer nanostructure by constituting a carbonaceous nuclear core, and a fluorine-bearing cationic polymer film surface [66]. Moreover, in another study, Luo et al. (2018) fabricated F-doped CQDs by combining ring-opening polymerization-dehydrative carbonization (RPDC) process and hydrothermal method (12 h at 180 °C), while utilizing PEI 600Da and 2,2,3,3,4,4-hexafluoro-1,5-pentanediol diglycidyl ether (as F source) as starting materials [67]. The maximum excitation and emission wavelengths of these F-doped CQDs are found to be 348 and 460 nm, respectively, with QY of 5.6%.
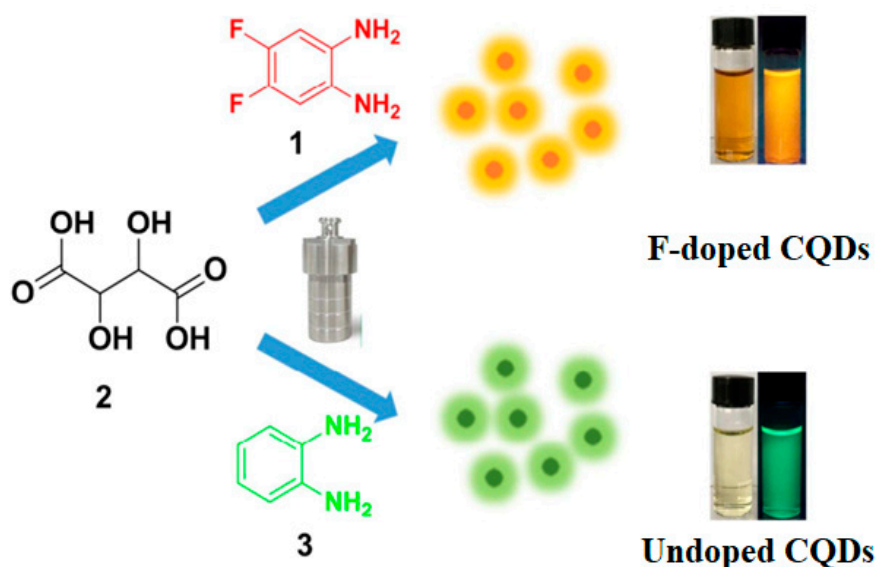
Figure 1. Synthesis of F-doped carbon quantum dots (CQDs) and un-doped CQDs via hydrothermal method. Reproduced with permission from Zuo et al. [65] Copyright ACS, 2017.

2.2.3. N-Doped CQDs

At first, Liu et al. (2012) developed N-doped nanodots/CQDs with blue emission, via hydrothermal treatment (3 h at 180 °C) of a natural resource—i.e., grass, where they have observed a size–dependent QY variation (i.e., decrease in size from 22 to 2 nm resulted in increase in QY from 2.5 to 6.2%) [68]. Then, Dey et al. (2013) synthesized blue-light emitting CQDs with high N doping content of 18–22% via the reactions between glucose and urea under hydrothermal (1 h at 150 °C) and microwave (600 W for 7 min) conditions; however, they have resulted in QY of 0.7 and 1%, respectively [69]. In another study, Wang et al. have made N-doped CQDs with blue emission via an aqueous phase strategy—i.e., hydrothermal treatment (2 h at 150 °C)—by using folic acid as starting material, where these CQDs have possessed high photoluminescence QY of 23% [70]. Similarly, Niu et al. have employed glutamic acid as the major precursor to synthesize N-doped CQDs with blue emission and enhanced QY of 28% via pyrolysis method at 200 °C, where nitrogen and carbon atoms might have simultaneously decomposed from glutamic acid to form these CQDs [71]. In analogous fashion, Qian et al. have fabricated the N-doped CQDs with blue emission and QY in the range of 9.8–36.3% via optimized solvothermal reaction (0.5, 1, and 2 h at 200 °C) between carbon tertrachloride (CCl$_4$, as C source) and diamines—e.g., 1,2-ethylenenediamine, 1,3-propanediamine, or 1,4-butanediamine (as N source), used at different ratios (2:1, 1:1, 1:2, and 1:3) [72]. Herein, the QY of these CQDs is not correlated with their N content and this could be due to the difference in the ratios of pyridinic to pyrolic N atoms in the samples, where only pyrolic nitrogen atoms have participated in the protonation process. Moreover, Zhang et al. [73] and Campos et al. [74] have made N-CQDs with blue emission using precursors such as dried monkey grass and lactose, respectively, via a hydrothermal process. In a similar way, Lv et al. have also developed N-doped CQDs via the hydrothermal method (5 h at 220 °C) by using ethylenediamine (as N dopant) and citric acid (as C source) as precursors [75]. In another study, Wu et al. have prepared N-rich metal-free CQDs or metal-doped CQDs with bright luminescence by hydrothermal method (20 h at 250 °C) and carbonization (as shown in Figure 2) using tetraphenylporphyrin (TPP) or its transition metal Pd(II) or Pt(II) complex (as a C precursor) and ethylenediamine (as N precursor) [76]. All N-doped CQDs – i.e., CQDs, Pd-CQDs, and Pt-CQDs have displayed bright blue emission and typical excitation-dependent emission behavior, with QY of 10.1%, 17.8%, and 15.2%, respectively. However, Hu et al. (2017) have used an efficient method to control the speciation of N-doping—i.e., pyridinic *N*, pyrrolic *N*, graphitic *N*, and amino *N*, by ferric ion catalysis (Fe^{3+} ions with increasing molar ratios of 10%, 20%, 30% and 40%) in the hydrothermal

reaction (4 h at 200 °C) of L-histidine [77]. This strategy have induced the following effects: (i) an increment of pyrrolic *N* (from 35.5% to 47.6%), and a decrement of pyridinic *N* (from 34.8% to 23.2%), and (ii) well-organized arrangement of graphic core and more N moieties exposed on the surface of N-doped CQDs. Consequently, the photoluminescence property (QY) of blue-light emitting N-doped CQDs has been improved from 6.2% to 27.0% with the increase in catalysis with Fe^{3+} ions.
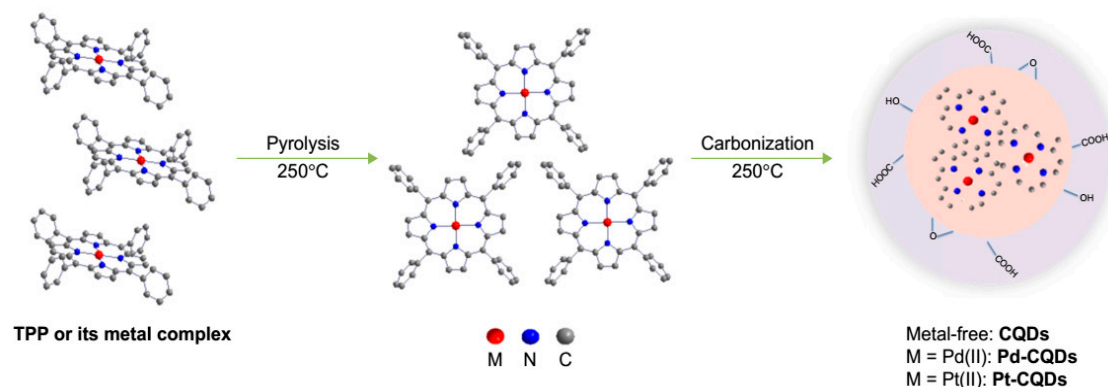

Figure 2. Schematic of the proposed formation procedure of CQDs and M-CQDs, where CQDs, carbon quantum dots; M-CQDs, metal-doped CQDs; TPP, tetraphenylporphyrin. Reproduced with permission from Wu et al. [76] Copyright Dovepress, 2017.

In a recent investigation, Ding et al. introduced a novel precursor (PVP) and effectively prepared N-doped and 10-trioxa-1,13-tridecanediamine (TTDDA)-passivated CQDs that have displayed multi-color emission and improved QY of 19.6% (via pyrolysis at 400 °C), while reducing the reaction time and production of toxic volatile by-products [78]. The reason behind the QY improvement via N-doping is ascribed to the newly created luminescent centers, via trapping of the radiative electron–hole pairs—ascribed to the disorders generated in the carbon hexagonal rings due to the nitrogen bonding with the carbon atoms. Similarly, Wang et al. have also investigated the effects of the usage of C sources having different carboxyl groups—i.e., glycolic acid, malic acid, and citric acid—on the synthesis of N-doped CQDs via hydrothermal method (1 h at 250 °C), where urea acted as the N-doping precursor [79]. These N-doped CQDs have displayed blue, cyan, and green fluorescence, respectively; moreover, it has been found that more amino groups have been conjugated to the surface of the N-doped CQDs, which are prepared by using the C sources with large number of carboxyl groups (i.e., glycolic acid < malic acid < citric acid).

In another study, Jiang et al. have prepared N-doped CQDs by using 1,2,4-triaminobenzene as both C and N sources (self-doping) in hydrothermal process (12 h at 120 °C) [80]. Similarly, Ji et al. have also used only one precursor—i.e., polyacrylamide (as both C and N sources—self-doping) solution to prepare N-doped CQDs via hydrothermal reaction (24 h at 260 °C) [81]. In another study, Xu et al. have used only tribute chrysanthemum flowers as the novel C and N precursors (self-doping) to prepare N-doped CQDs with QY of 17.3% via hydrothermal pyrolysis method (24 h at 180 °C) [82]. Recently, Jiang et al. have utilized Ginkgo leaves as both C and N sources (self-doping) to produce N-doped CQDs with improved QY of 22.8% via hydrothermal method (10 h at 200 °C) [83]. Analogously, Wang et al. have synthesized N-doped CQDs with enriched QY of 30.7% by using m-aminobenzoic acid as the only precursor via hydrothermal method (12 h at 180 °C), where the NH_2 groups of the precursor is used as N source to dope the CQDs (self-doping) [84].

In an investigation, Wu et al. synthesized N-doped CQDs with enhanced QY of 51% via hydrothermal method (11 h at 230 °C) by using ethylenediamine as N dopant, and a non-toxic C source—i.e., microcrystalline cellulose (consisting of 1,4-anhydro-D-glucopyranose units) [85]. However, Hou et al. fabricated N-doped CQDs with enhanced QY of 73.2% via solid-phase thermal treatment (1.5 h at 170 °C) of citric acid (as C source) and dicyandiamide (as N source) [86]. In another study, Zhu et al. have prepared N-doped CQDs with higher QY of 80% via hydrothermal

reaction of citric acid (as C source) and ethylenediamine (as N dopant), while optimizing their reaction temperatures at 150, 200, 250, and 300 °C for 5 h [87]. Lately, Tang et al. have achieved an enhanced QY of 84.1% for the N-doped CQDs that are synthesized in less than 8 min using precursors of ethylenediamine (as N dopant) and citric acid (as C source), via a microreactor (with reaction temperature of 150–230 °C) in the presence of foamy copper (having different porosities—50–98%) embedded in a microchannel—as shown in Figure 3 [88]. Zheng et al. have developed thermal pyrolysis route (0.5 h at 170 °C) to prepare N-doped CQDs with improved QY of 88.6% using citric acid and diethylenetriamine as the precursor materials [89]. However, recently, Meiling et al. reported N-doped CQDs with the highest QY of 90% after optimizing the following parameters: (i) the precursors (including N additives like Tris, urea and ethylenediaminetetraacetic acid, and carboxylic acid based C sources including 1,2,3,4-butanetetracarboxylic acid, acetic acid, citric acid, malonic acid, oxalic acid, and succinic acid) and its concentration/composition; (ii) reaction time; and (iii) excitation wavelength and pH dependence of the photophysical properties of N-doped CQDs [90].
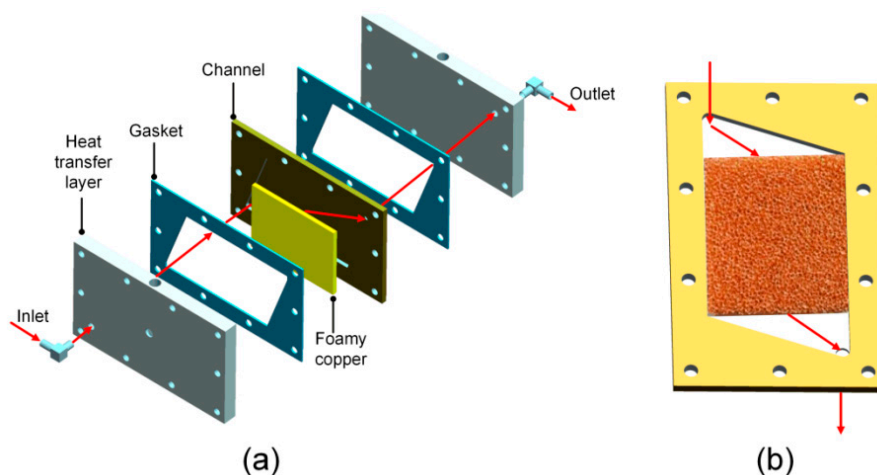

Figure 3. (**a**) Schematic diagram of the microreactor, and (**b**) enlarged view of the microchannel reaction. Reproduced with permission from Tang et al. [88] Copyright Elsevier, 2018.

2.2.4. P-Doped CQDs

Zhou et al. (2014) have proposed that phosphorous, behaving as an n-type donor, can form substitutional defects in CQDs, and thereby can modify their luminescence properties [91]. Based on this, they have synthesized P-doped CQDs via solvent-thermal reaction (on different reaction time periods of 1, 3, 5, and 9 h at 200 °C) between phosphorous tribromide (as P source) and hydroquinone. Herein, P doping in CQDs have induced strong blue emission (with QY of 25.1%) in comparison to un-doped/prisitine CQDs (with QY of 3.4%), as shown in Figure 4. This fluorescence enhancement could be due to the increased band gap into UV-Vis region ascribed to the coexistence of defect-sites and isolated sp^2 carbon clusters (caused by the addition of phosphorus in P-doped CQDs)—giving rise to stronger visible fluorescence than the existence of single sp^2 carbon clusters (in pristine CQDs). In another study, Shi et al. (2015) have prepared P-doped CQDs with blue emission and QY of 21.8% by hydrothermal treatment (5 h at 200 °C) of sucrose and phosphoric acid [92]. However, Sarkar et al. (2015) have synthesized P-doped CQDs with green emission by using thermal coupling between citric acid and Na-salt of glycine, L-valine, and L-isolucine in the presence of sodium dihydrogen phosphate (as P source) [93]. Moreover, these P-doped CQDs using glycine, L-valine, and L-isolucine displayed higher QYs (i.e., 15.2%, 11.0% and 19.7%) as compared to their un-doped CQDs (i.e., 8%, 8.9% and 3.7%), respectively. Analogously, Li et al. (2017) reported aggregation-induced red shift emission (from 455 to 595 nm by modifying the solution concentration) for the as-synthesized P-doped CQDs synthesized via hydrothermal reaction (12 h at 200 °C) between concentrated phosphoric acid and triethylphosphonoacetate [94]. The possible reasons behind the resulting red shift in the emission

wavelength are the formation of (i) an electron rich system inside P-doped CQDs ascribed to the doping with the electron-rich phosphorus, and also (ii) an extended electron system attributed to the increase in the particle sizes (due to the aggregation). Recently, Chen et al. (2018) synthesized P-doped CQDs with QY of 1.3% by simply mixing L-threonine, phosphorus pentoxide (as P source), and water [95]. However, Yang et al. (2018) synthesized eco-friendly P-doped CQDs (with QY of 3.5%) via hydrothermal treatment (4 h at 160, 200 or 240 °C) of phytic acid and sodium citrate [96]. Herein, phytic acid is selected as P source due to its hexatomic ring structure with rigid C-P bonds, abundant phosphate group and completely natural, which resulted in improved—i.e., 8.52 wt.%—P content in the as synthesized CQDs. However, Wang et al. (2018) made P-doped CQDs with improved QY of 21.65% by using microwave reaction (700 W for 10 min) between phytic acid (as the P-source) and ethylenediamine [97]. In addition to the above, Omer et al. enhanced the QY of the P-doped CQDs to 62% by chelating them with certain metal ions (for instance Al^{3+}), where these P-doped CQDs are prepared using low temperature solvothermal reaction between lactose (as C source) and phosphoric acid (as P source) [98].
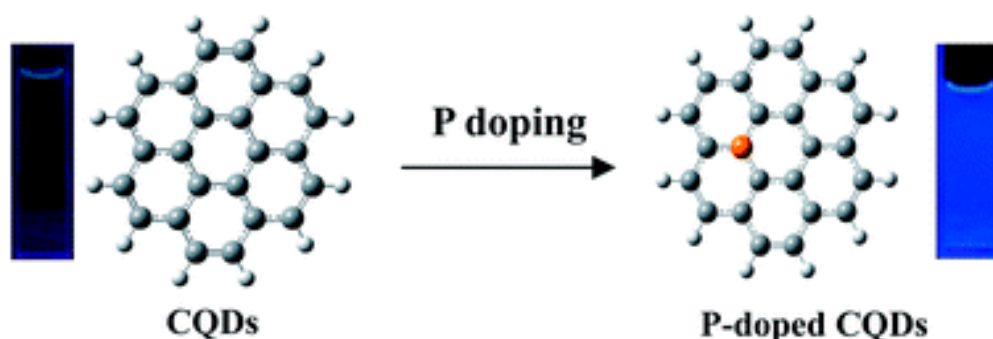

Figure 4. Schematic diagram of P-doping in the CQDs and corresponding changes in the fluorescence property. Reproduced with permission from Zhou et al. [91] Copyright RSC, 2014.

2.2.5. S-Doped CQDs

Initially, Chandra et al. (2013) prepared sulphur modified CQDs (i.e., S-doped CQDs)—which exhibited QY of 11.8% and blue emission—while using sulfuric acid and thiomalic acid as starting materials [99]. Then, Hu et al. (2014) demonstrated the first use of waste frying oil as the major precursor for the synthesis of S-doped CQDs (with blue emission/QY of 3.66%) via carbonization using concentrated sulfuric acid due to their strong dehydrating and oxidizing properties [100]. Moreover, the as-synthesized S-doped CQDs have displayed partial disordered graphite-like structure, where the S-doping have opened a wide band gap of 3.28 eV in CQDs, initiating an intense UV emission of 378 nm. Furthermore, these S-doped CQDs have possessed a distinct pH-sensitive photo luminescence in the pH range from 3–9. Similarly, Xu et al. (2015) have prepared S-doped CQDs with blue emission using hydrothermal reaction (6 h at different reaction temperatures of 160, 180, 200, 220 and 240 °C) of sodium citrate and sodium thiosulfate (at 1:3 ratio), where the resultant CQDs have exhibited significantly high QY of 67% [101]. Moreover, they also showed stable fluorescent intensity for S-doped CQDs in wide range of pH (i.e., from 6 to 10).

Later, Rahmayanti et al. (2015) produced yellowish green emission based S-doped CQDs by simple heating process of sulphur deposits, citric acid and urea [102]. Lately, Yang et al. (2017) fabricated S-doped CQDs and their derivatives—referred to as three-dimensional (3D) carbon nanoflowers; S-CNFs—with emission/QYs of blue/4% and green/6.4%, respectively, by using a simple heating process (10 and 30 min at 200 °C) of 5-sulfosalicylic acid dihydrate and diethylene glycol [103]. Moreover, Travlou et al. (2017) obtained two different S-doped CQDs with QY of 9% and 6%, by using 2 different S containing polymer precursors (i.e., poly(sodium4-styrene sulfonate) and poly(4-styrene sulfonicacid co-maleic acid), respectively via hydrothermal method(6 h at 200 °C) [104]. Similarly, Loukanov et al. (2018) developed S-doped CQDs with blue emission and QY of ~49% via microwave-assisted-pyrolysis

(600 W for 3 min) of mixtures of citric acid and cysteamine [105]. Recently, Pawar et al. (2018) carried out low cost and quick synthesis of S-doped CQDs via acidic carbonization of sucrose and sulphuric acid without using any sophisticated instrument, where the resultant CQDs have shown QY of 5.77% [106]. In another latest study, Wu et al. (2018) used Vitamin B1 (thiamine hydrochloride, as the S source) and ethylenediamine (as shown in Figure 5) to effectively prepare S-doped CQDs with blue emission and QY of 4.4% via hydrothermal strategy (12 h at 200 °C) [107].
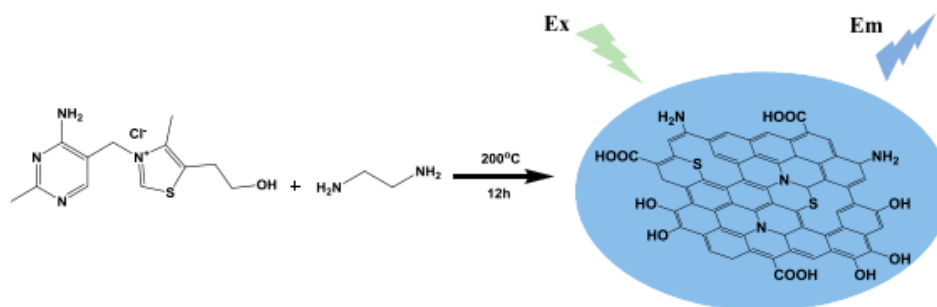

Figure 5. Schematic diagram of the synthesis of S-doped CQDs via hydrothermal reaction. Reproduced with permission from Wu et al. [107] Copyright Elsevier, 2018.

2.3. Co-Doped CQDs

2.3.1. B, N Co-Doped CQDs

Liu et al. prepared blue-emitting B and N co-doped CQDs—from hydrothermal reaction (8 h at 220 °C) of branched polyethylenimine (PEI) and 4-formylphenylboronic acid, where these co-doped CQDs have showed (i) QY of 15.85% and (ii) temperature (27–90 °C) and pH (3–13) dual responses [108]. In another similar study, Ye et al. prepared three different blue-emitting B and N co-doped CQDs via hydrothermal method (4 h at 160 °C) by using citric acid anhydrous, ethylenediamine, and three different kinds of borate—i.e., sodium tetraborate, boric acid, and manganese borate, which resulted in a respective QY of 29.01%, 51.42%, and 68.28% [109].

In an investigation, Guo et al. synthesized B and N co-doped CQDs with yellow-green emission and QY of 6.59% via hydrothermal method (12 h at 180 °C) using 2-hydroxyphenylboronic acid and ethylenediamine as the starting materials—(as shown in Figure 6), where these CQDs have displayed better stability in aqueous solution with high ionic strength (0.25–1.2 M of NaCl) and different pH of 3–13 [110]. However, Huang et al. synthesized B and N co-doped CQDs with green emission and improved QY of 47% via hydrothermal method (7 h at 160 °C) by using 3-aminobenzeneboronic acid and 1,2-ethylenediamine as precursors [111]. Moreover, the fluorescence intensity of these CQDs has not modified even under constant UV irradiation at 365 nm for about 150 min, ultrahigh concentration of NaCl solution and a wide range of pH values (3–11).
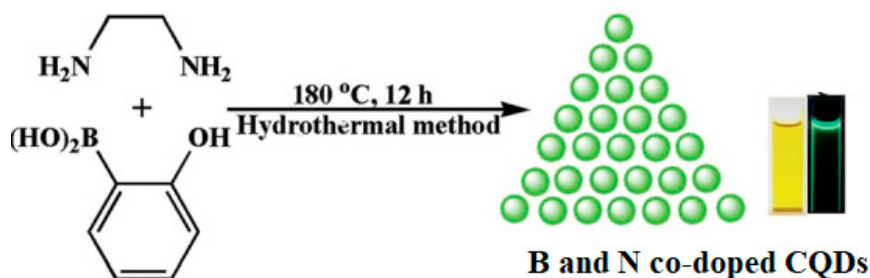

Figure 6. Schematic diagram of the synthesis of B and N co-doped CQDs via hydrothermal reaction. Reproduced with permission from Guo et al. [110] Copyright RSC, 2017.

Recently, Xiao et al. synthesized different B and N co-doped CQDs with blue emission (using self-doping method) from three distinct aminophenylboronic acid isomers based precursors (including 2-aminophenylboronic acid, 3-aminophenylboronic acid monohydrate, and 4-aminophenylboronic acid hydrochloride) via hydrothermal method (8 h at 160 °C) [112,113]. Herein, 3-aminophenylboronic acid monohydrate based CQDs have displayed better photoluminescence with QY of 7%, and stable towards (i) a broad range of pH (3–12) and (ii) a continuous UV irradiation of 45 min. In another study, Tian et al. have utilized 3-aminophenylboronic acid as the main and only precursor (self-doping) to synthesize B and N co-doped CQDs with QY of 25.9% through hydrothermal method (4 h at 180 °C) [114]. Herein, these CQDs have possessed stable fluorescence emission (i) at a wide range of pH (i.e., 2–14), and (ii) under continuous UV irradiation in ambient and high ionic strength conditions.

2.3.2. B, S Co-Doped CQDs

In a study, Zhao et al. have synthesized B and S co-doped CQDs with blue emission and QY of 25.7%, via hydrothermal synthesis (8 h at 200 °C) by using borax and poly (sodium-p-styrenesulfonate) as the major B and S sources [115]. Herein, maximum excitation and emission wavelengths of these CQDs are observed at about 250 and 308 nm, respectively. Moreover, a large blue shift in emission for B and S co-doped CQDs was also observed, which was attributed to the strong electron-withdrawing ability of boron.

2.3.3. F, N Co-Doped CQDs

Yang et al. demonstrated the synthesis of F and N co-doped CQDs with yellow light emission via one-step microwave-assisted carbonation route (750 W for 5 min) [116]. Herein, they disclosed that the doping of F atoms has led to an improved π-electron system inside the core of the CQDs, which consequently resulted in the red-shifts in the photoluminescence emission under the excitation at 530 nm.

2.3.4. N, P Co-Doped CQDs

Omer et al. prepared blue emitting N and P doped CQDs with 0.41% of QY, via hydrothermal method (15 h at 180 °C) by using four major components as precursors including trimesic acid, urea, polyethylene diamine branched, and ortho-phosphoric acid [117]. However, Huang et al. applied a low-temperature heating (50 min at 80 °C) strategy to make N and P co-doped CQDs with blue emission and enhanced QY of 12.7%, while using sucrose as C source, and 1,2-ethylenediamine and phosphoric acid as N and P dopants [118]. Moreover, these co-doped CQDs have exhibited excellent fluorescent stability over broad range of pH (4–11), ultra-high ion strength (3 M KCl), and constant UV light irradiation (for 3 h). Analogously, Liao et al. have also prepared N and P co-doped CQDs that have emitted blue fluorescence with better QY of 15.4%, while using pyridoxal 5-phosphate and ethanediamine as precursors in hydrothermal protocol (4 h at 180 °C) [119]. Li et al. have prepared N and P co-doped CQDs by microwave-assisted thermolysis (700 W for 7 min) of N-phosphonomethyl aminodiacetic acid and ethylenediamine, where these co-doped CQDs have exhibited (i) bright blue fluorescence with improved QY of 17.5% and (ii) pH-dependent fluorescence [120]. Recently, Chandra et al. have made highly fluorescent blue emitting N and P co-doped CQDs in two different studies with QY of 59% and 10.58% via hydrothermal reaction of citric acid and diammonium phosphate (at 1:4 ratio) [121,122].

In an investigation, Liu et al. made green emitting N and P co-doped CQDs with QY of 9.59% while using glucose as the C source, 1,2-ethylenediamine as N-dopant and concentrated phosphoric acid as P-dopant in acid-base neutralization spontaneous heat based synthesis method [123]. Moreover, these CQDs displayed better luminescence stability under a 365 nm UV lamp irradiation about 5 h, and over wide range of pH (3–10). Analogously, Omer et al. modified the precursors (such as citric acid, urea and phosphoric acid in dimethylformamide solution) in hydrothermal process (24 h at 180 °C) and prepared green-yellowish emitting N and P co-doped CQDs with improved QY of 15% [124]. Similarly

Li et al. designed and prepared green emitting N and P co-doped CQDs by using hydrothermal process (5 h at 200 °C) of the molecular precursors such as diethylenetriaminepenta(methylenephosphonic acid) and m-phenylenediamine and (as shown in Figure 7) [125]. The as-synthesized CQDs displayed (i) QY of 32% and (ii) significantly enhanced photo-stability in a wide range of pH (2–10) values. In another study, Yang et al. synthesized similar CQDs with green emission and equivalent QY by using the same precursors [126]. Moreover, Sun et al. generated N and P co-doped CQDs via microwave heating (800 W for 40 s) of the precursors including m-phenylenediamine, ethylenediamine, and ortho-phosphoric acid (taken in the stoichiometric ratio of 1:3.2:1.6) in water at ambient pressure [127]. These co-doped CQDs have exhibited bright dual blue (centered at 450 nm/QY of 51%), and green (centered at 510 nm/QY of 38%) emission bands.
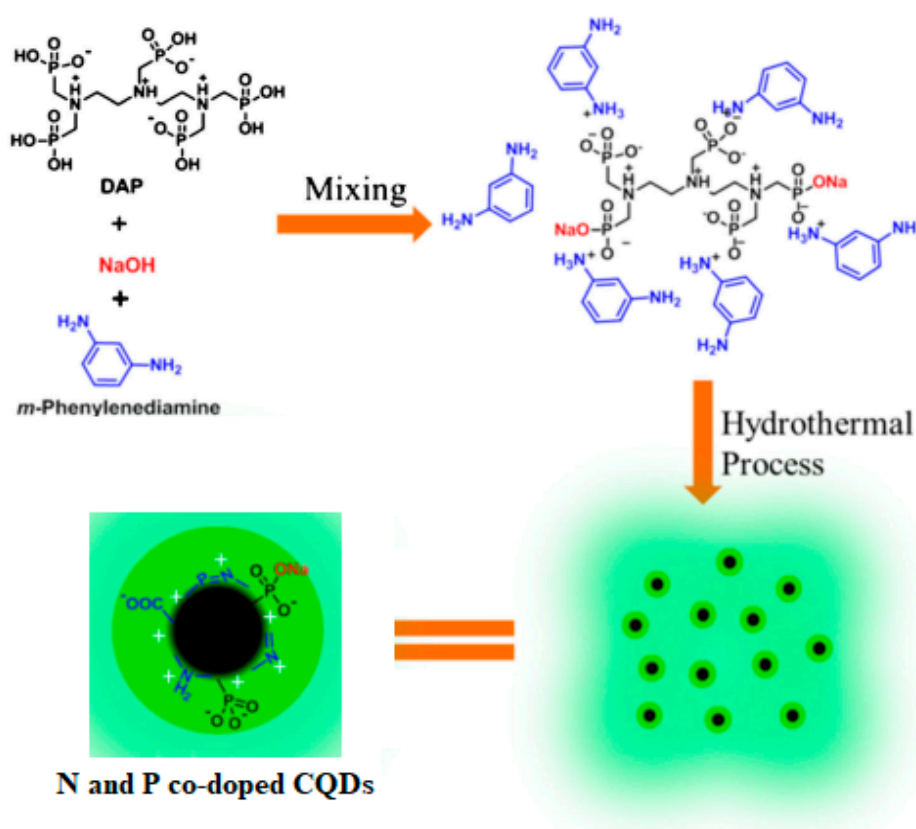

Figure 7. Schematic diagram of the synthesis of N and P co-doped CQDs via hydrothermal method. Reproduced with permission from Li et al. [125] Copyright Springer-Verlag Wien, 2017.

Bao et al. used a simple strategy towards the synthesis of three different N and P co-doped CQDs via hydrothermal treatment of a single precursor—i.e., Eleocharis dulcis juice (self-doping) by making adjustments in the reaction temperatures (5 h at 90, 120, 150 °C), which correspondingly resulted in (i) QYs of 3.3, 11.2, and 8.6%, and (i) fluorescence emission of distinct colors including navy blue, blue, and cyan [128]. In another study, Gong et al. conveniently prepared N and P co-doped CQDs by carbonization of only one precursor (self-doping)—i.e., adenosine-5′-triphosphate (ATP))—via hydrothermal treatment (2 h at 300 °C) [129]. These co-doped CQDs (i) have emitted blue luminescence with QY up to 23.5% and (ii) possess strong and stable fluoresce over a wide range of pH values (4–13) and ionic concentrations up to 400 mM NaCl. In a similar investigation, Shamsipur et al. used self-doping method to develop N and P co-doped CQDs with bright blue luminescence and improved QY of 35%, by using an aqueous solution of alendronate sodium (utilized as both N and P source) via hydrothermal method (20 h at 180 °C) [130].

2.3.5. N, S Co-Doped CQDs

N and S co-doped CQDs—with blue emission and QY of 2.36%—were synthesized by Hu et al. by utilizing microwave-assisted pyrolysis (800 W for 30 min) of the precursors rice (as C source) and N-acetyl-L-cysteine (NAC) as both N and S dopant [131]. Moreover, the effect of different mass ratios of NAC to rice (i.e., NAC/rice—0.20, 0.40, 0.60, and 0.80) on the co-doped CQDs has been also investigated with the assistance of high-performance liquid chromatography coupled with fluorescence detection, where higher NAC/rice ratio has benefited the generation of CQDs with stronger fluorescence emission. In another study, Akhgari et al. prepared N and S co-doped CQDs from pomegranate juice (that served as the C source), and L-cysteine (that provided N and S) via hydrothermal method (5 h at 120 °C), where these CQDs have exhibited blue fluorescence and QY of 4.8% [132]. Analogously, Cheng et al. fabricated N and S co-doped CQDs with blue emission and QY of 13.3% by combustion treatment of cellulose-based biowaste of willow catkin soaked in N/S aqueous solution containing urea and sulfuric acid (98%), where the possible mechanism involved in the synthesis of these CQDs is shown in Figure 8 [133]. Moreover, Simoes et al. synthesized N and S co-doped CQDs via microwave (700 W for 5 min) reaction of citric acid, urea and sodium thiosulfate (in the proportion of 1:1:3)—utilized as C, N and S sources, respectively [134]. Furthermore, Wang et al. have synthesized N and S co-doped CQDs with blue emission and QY of 16% through hydrothermal reaction (6 h at 200 °C) of thiourea, urea, and sodium citrate [135].

Figure 8. Schematic diagram of the synthesis of N and S co-doped CQDs via combustion process from cellulose-based biowaste willow catkin. Reproduced with permission from Cheng et al. [133] Copyright Elsevier, 2019.

In another similar investigation, Chen et al. utilized garlic to make CQDs with blue emission and QY of 13% via hydrothermal method (10 h at 180 °C), where the as-prepared CQDs were doped with N and S in the format of pyridinic-N, pyrrolic-N and thiophene-S [136]. Analogously, Zhao et al. prepared N and S co-doped CQDs with blue emission and QY of 17.5% from garlic by hydrothermal method (3 h at 200 °C) [137]. In similar fashion, Sun et al. used garlic as precursor to prepare blue emitting N and S co-doped CQDs via hydrothermal method (6 h at 200 °C), where ethylenediamine (1 ml) is introduced during synthesis to enhance the QY from 5.1 to 20.5% [138]. Moreover, it can be noted that, regardless of the same precursor, the QY (13%) of the N and S co-doped CQDs prepared by

Chen et al. is slightly lower than the QY of Zhao et al. (17.5%) and Sun et al. (20.5%), which is mainly attributed to their lower reaction temperature.

In another study, Chen et al. prepared N and S co-doped CQDs with blue emission via hydrothermal treatment (6 h at 160 °C) of citric acid and cystamine dihydrochloride, where these CQDs have exhibited excellent excitation-wavelength-independent photoluminescence property and QY of 39.7% in comparison to only N-doped CQDs (QY = 2.6%) prepared using citric acid and 1,6-diaminohexane dihydrochloride as the precursors [139]. In similar fashion, Ding et al. synthesized blue emitting N and S co-doped CQDs with QY of 54.4% via hydrothermal reaction of α-lipoic acid (as C and S source), sodium hydroxide and ethylenediamine (as N source), while optimizing the reaction time period of 1, 3, 7, 11, 15, and 19 h at 250 °C [140]. Moreover, it has been found out that (i) C = O groups on the surface of the CQDs surface are considered to be the main emission centers for blue luminescence, (ii) C=N & C–N bonds in the form of polyaromatic structure are majorly promoting the fluorescence, and (iii) the co-doping of sulphur is found to be synergistic for nitrogen doping in co-doped CQDs.

Similarly, Liao et al. directly synthesized N and S co-doped CQDs from citric acid and thiamine hydrochloride via hydrothermal protocol (5 h at 160 °C), resulting in blue emission and better QY of 63.8% [141]. Dong et al. used citric acid (as C source) and l-cysteine (as both N and S source) to produce N and S co-doped CQDs with violet-blue emission and high QY of 73% through hydrothermal treatment (3 h at 200 °C) [142]. Analogously, Anjana et al. fabricated N and S co-doped CQDs with blue emission and high QY of 78 ± 10% via microwave assisted route (700 W for 40 s) by using citric acid as C source and l-cysteine as a source of N and S—(as shown in Figure 9) [143]. Moreover, the influence of pH (from 1 to 11) towards the fluorescence intensity is also monitored, where the fluorescence intensity of these CQDs has increased with the decrement in pH and maximum fluorescence is observed at synthesized pH 2.5. The pH dependent fluorescence in N and S co-doped CQDs is mainly due to the three possible prototropic equlibria—(i) phenol↔phenolate, (ii) carboxylic ↔ carboxylate, and (ii) ammonium ↔ amine ion that occurred in those CQDs.

Figure 9. Schematic diagram of the synthesis of N and S co-doped CQDs via microwave process. Reproduced with permission from Anjana et al. [143] Copyright Springer-Verlag GmbH Austria, part of Springer Nature, 2017.

Zhu et al. (2018) made green emitting N and S co-doped CQDs with QY of 5.7% by using the reaction between sodium lignosulfonate and p-phenylenediamine (as C/N/S sources) in solvothermal process (9 h at 200 °C) [144]. Analogously, Zhou et al. (2017) also prepared N and S co-doped CQDs via hydrothermal method (10 h at 200 °C), where these CQDs have possessed relatively enhanced QY of 43%, and also have presented unique optical properties with dual-emission (blue and yellow) under single excitation wavelength [145]. Herein, the blue emission is due to the surface energy traps emission and the yellow emission is ascribed the intrinsic state emission. Similarly, Das et al. (2018) synthesized green emitting N and S co-doped CQDs with enhanced QY 69.27% by using Kappa carrageenan and urea as the major precursors in hydrothermal method (5 h at 210 °C), while the optimizing precursor ratio (carrageenan: urea), reaction temperature and reaction time [146].

Wei et al. (2019) used a single precursor—Allium fistulosum (self-doping) to generate N and S co-doped CQDs with blue emission and QY of 10.48% through hydrothermal treatment (3 h at 220 °C) [147]. In another analogous investigation, Xu et al. (2017) converted the biomass—Enteromorpha prolifera (algae genera for green tide)—to N and S co-doped CQDs (via self-doping) with blue emission and QY of 12.3% via hydrothermal method, while optimizing the effects of the reaction time (i.e., 3, 6, or 10 h at 180 °C) [148]. Similarly, Zhao et al. (2018) have also used a single precursor—glutathione (self-doping) to prepare N and S co-doped CQDs in hydrothermal process (6 h at 200 °C), where the resultant CQDs have exhibited blue emission and QY of 17.5% [149]. In another study, Xu et al. (2017) used only casein (self-doping) as C, N, and S sources in pyrolysis strategy (4 h at 180 °C) to synthesize blue emitting N and S co-doped CQDs with QY of 31.8% [150]. Ye et al. (2017) synthesized different N and S co-doped CQDs (through self-doping) with blue emission via the pyrolysis carbonization (3 h at 300 °C) of diverse precursors—i.e., feathers, egg white, egg yolk, and manure from pigeon, resulting in QYs of 24.87%, 17.48%, 16.34%, and 33.50% correspondingly [151]. Herein, feather and eggs are majorly chosen for the synthesis purpose as they are rich in (i) C, N, S, and O due to its composition of β-keratin, and (ii) proteins, carbohydrate, and fat that contain a lot of heteroatoms (N and S), respectively.

Moreover, different doped/co-doped CQDs along with their synthesis method, reaction conditions, QY and corresponding applications are summarized in Table 1.

Table 1. Doped and co-doped CQDs along with their synthesis method, precursors, reaction conditions, quantum yield (QY), and applications.

Synthesis Method	Precursors	Reaction Conditions	Color	QY (%)	Applications	Reference
Boron (B)-Doped CQDs						
Solvothermal	Hydroquinone and boron tribromide	2 h at 200 °C	Blue	14.8	Detection of hydrogen peroxide (H_2O_2) and glucose (LOD of 8 μM)	[61]
Microwave	Citric acid, urea, and boric acid	700 W for 4 min	Green	15	-	[62]
Hydrothermal	Ascorbic acid and boric acid/sodium borohydride/sodium borate/borax	7 h at 200 °C	-	2.1–5.4	Detection of iron (Fe^{3+}) (LOD of 3.1 nM) ions and ascorbic acid (LOD of 30 nM)	[63]
Hydrothermal	Phenylboronic acid	10 h at 200 °C	-	12	Detection of potassium sorbate (LOD of 6.1 nM), and vitamin B12 (LOD of 8 nM) in mineral water, vinegar, bread, vitamin drink, and VB12 tablets.	[64]
Fluorine (F)-Doped CQDs						
Solvothermal	Citric acid and 4,5-difluorobenzene-1,2-diamine	8 h at 180 °C	Yellow	31	Detection of intracellular Ag^+ and cell imaging (HEK 293 and B16F10 cell lines)	[65]
Solvothermal	Tetrafluoroterephthalic acid (TFTA) and 1.8K branched polyethyleneimine (1.8K b-PEI)	6 h at 180° C	Green	-	Gene delivery	[66]
Hydrothermal	PEI 600Da and 2,2,3,3,4,4-hexafluoro-1,5-pentanediol diglycidyl ether	12 h at 180 °C		5.6	Gene delivery and cell imaging (HeLa and 7702 cell lines)	[67]
Nitrogen (N)-Doped CQDs						
Hydrothermal	Grass	3 h at 180 °C	Blue	2.5–6.2	Label-Free Detection of Cu (II) ions (LOD of 1 nM)	[68]
Hydrothermal	Glucose and urea	1 h at 150 °C	Blue	0.7	White light emission	[69]
Microwave		600 W for 7 min		1		
Hydrothermal	Folic acid	2 h at 150 °C	Blue	23	Cell imaging (U87 cell line)	[70]
Pyrolysis	Glutamic acid	5 min at 200 °C	Blue	28	Detection of anti-bacterial drug—amoxicillin	[71]
Solvothermal	Carbon tertrachloride and diamines—e.g., 1,2-ethylenenediamine, 1,3-propanediamine, or 1,4-butanediamine at different ratios of 2:1, 1:1, 1:2, and 1:3	0.5, 1 and 2 h at 200 °C	Blue	9.8–36.3	Detection of Ag^+, Fe^{3+}, and hydrogen peroxide (H_2O_2)	[72]
Hydrothermal	Dried Monkey grass	6 h at 180° C	Blue	-	Detection of iodide (I^-) ions (LOD of 3.7 μM)	[73]
Hydrothermal	Lactose	3 h at 180 °C	Blue	10.75	Detection of pyridine (LOD of 0.03 mM)	[74]
Hydrothermal	Citric acid and ethylenediamine	5 h at 220 °C	Blue	-	Detection of Fe^{3+} (LOD of 79 nM) ions	[75]

Table 1. *Cont.*

Synthesis Method	Precursors	Reaction Conditions	Color	QY (%)	Applications	Reference
			Nitrogen (N)-Doped CQDs			
Hydrothermal	Tetraphenylporphyrin or its transition metal Pd(II) or Pt(II) complex and ethylenediamine	20 h at 250 °C	Blue	10.1, 17.8, and 15.2	Detection of Fe^{3+} (LOD of 3.7 µM) ions in aqueous solution and cells, and cell imaging (HeLa cell line)	[76]
Hydrothermal	L-histidine	4 h at 200 °C	Blue	27	Detection of Fe^{3+} (LOD of 1 µM/L) ions	[77]
Pyrolysis	Polyvinyl pyrrolidone (PVP, K-30)	3 h at 400 °C	Blue	19.6	Multicolor cell imaging (HeLa cell line)	[78]
Hydrothermal	Glycolic-/malic-/citric-acid and urea	1 h at 250 °C	Blue, cyan, and green	-	Cell imaging (human osteogenesis sarcoma MG-63 cells)	[79]
Hydrothermal	1,2,4-triaminobenzene	12 h at 120 °C	Yellow	32.5	Bifunctional detection of Ag^+ (LOD of 0.20 µM) ions and cysteine (Cys) (LOD of 0.25 µM), and cell imaging (MCF-7 cell line)	[80]
Hydrothermal	Polyacrylamide	24 h at 260 °C	-	-	Detection of glucose (LOD of 0.25 mM) in serum samples	[81]
Hydrothermal pyrolysis	Tribute chrysanthemum flowers	24 h at 180 °C	Blue	17.3	Label-free detection of Fe^{3+} ions (LOD of 0.001 M) and hydrazine	[82]
Hydrothermal	Ginkgo leaf	10 h at 200 °C	Blue	22.8	Label-free detection of salazosulfapyridine (LOD of 40 nmol/L) in mouse plasma	[83]
Hydrothermal	m-aminobenzoic acid	12 h at 180 °C	Blue	30.7	Detection of Fe^{3+} ions (LOD of 0.05 µM) and pH	[84]
Hydrothermal	Microcrystalline cellulose and ethylenediamine	11 h at 230 °C	Blue	51	Detection of Fe^{3+} ions (LOD of 0.21 nM) in an acidic environment	[85]
Solid-phase thermal treatment	Citric acid and dicyandiamide	1.5 h at 170 °C	Yellowish-green	73.2	Label-free probe for detection of Fe^{3+} (LOD of 50 nM/L) and fluorine (LOD of 75 nM/L) ions	[86]
Hydrothermal	Citric acid and ethylenediamine	150, 200, 250 and 300 °C for 5 h	Blue	80	Multicolor patterning for anti-counterfeit applications, detection of Fe^{3+} ions (LOD of 1ppm) and cell imaging	[87]
Microreactor with foamy copper having different poriness values	Citric acid and ethylenediamine	8 min at 150–230 °C	Blue	84.1	Detection of Hg^{2+} ions (LOD of 2.104 nM)	[88]
Thermal pyrolysis	Citric acid and diethylenetriamine	0.5 h at 170 °C	Blue	88.6	Detection of chromium (VI) ions and ascorbic acid	[89]
Microwave	Carboxylic acids including 1,2,3,4-butanetetracarboxylic acid/acetic acid/citric acid/malonic acid/oxalic acid/succinic acid, and tris/urea/ethylenediaminetetraacetic acid	5−45 min at 200−230 °C	Blue	90	-	[90]

Table 1. *Cont.*

Synthesis Method	Precursors	Reaction Conditions	Color	QY (%)	Applications	Reference
Phosphorus (P)-Doped CQDs						
Solvent-thermal reaction	Hydroquinone and phosphorous tribromide	1, 3, 5 and 9 h at 200 °C	Blue	25.1	Cell imaging/biolabeling (HeLa cell line)	[91]
Hydrothermal	Sucrose and phosphoric acid	5 h at 200 °C	Blue	21.8	Detection of explosive—2,4,6-trinitrophenol (LOD of 16.9 nM)	[92]
Thermal coupling	Citric acid and Na-salt of glycine, L-valine and L-isolucine in the presence of sodium dihydrogen phosphate	2 h at 200 °C	Green	15.2, 11 and 19.7	Cell imaging (HeLa cell line)	[93]
Hydrothermal	Concentrated phosphoric acid and triethylphosphonoacetate	12 h at 200 °C	Blue or orange yellow	-	-	[94]
Simple mixing	L-threonine and phosphorus pentoxide	-	Blue	1.3	Detection of Au^{3+} (LOD of 5.86 μM), and L-methionine (LOD of 80 μM/L)	[95]
Hydrothermal	Sodium citrate and phytic acid	4 h at 160, 200 or 240 °C	Blue	3.5	Detection of Cu (II) ions (LOD of 1 nM)	[96]
Microwave	Ethylenediamine and phytic acid	700 W for 10 min	Green	21.65	Cell imaging/biolabeling (L929 cell line)	[97]
Solvothermal	Lactose and phosphoric acid	20–30 min at 80–90 °C	Yellow	62	Detection of Al^{3+} (LOD of 4 nM) and Zn^{2+} ions (LOD of 100 nM)	[98]
S-Doped CQDs						
Chemical process	Thiomalic acid and sulfuric acid	4 h at 90 °C	Blue	11.8	Solar cells, cell imaging (microbial strain of E. coli), and gene delivery	[99]
Carbonization	Waste frying oil and sulfuric acid	5 min at 100 °C	Blue	3.66	Cell imaging (HeLa cell line)	[100]
Hydrothermal	Sodium citrate and sodium thiosulfate	6 h at 160, 180, 200, 220, and 240 °C	Blue	67	Detection of Fe^{3+} ions (LOD of 0.1 μM)	[101]
Simple heating	Citric acid, urea and sulphur deposits	15 min at 225 °C	Yellowish green	-	-	[102]
Simple heating	Diethylene glycol and 5-sulfosalicylic acid dihydrate	10 min at 200 °C	Blue	4	Visible to near infrared fluorescent probes for hydrogen peroxide (LOD of 0.6 μM)	[103]
		30 min at 200 °C	Green	6.4		
Hydrothermal	Poly(sodium4-styrene sulfonate)	6 h at 200 °C	Blue	9	Detection of ammonia	[104]
	Poly(4-styrene sulfonicacid co-maleic acid)			6		
Microwave-assisted-pyrolysis	Citric acid and cysteamine	600 W for 3 min	Blue	49	Detection of calcium in hard water	[105]
Acid carbonization	Sucrose and sulphuric acid	-	Blue	5.77	Detection of Fe^{3+} ions (LOD of 0.56 μM) in highly acidic environment	[106]
Hydrothermal	Vitamin B1 (thiamine hydrochloride) and ethylenediamine	12 h at 200 °C	Blue	4.4	Detection of Fe^{3+} ions (LOD of 177 nM)	[107]

Table 1. *Cont.*

Synthesis Method	Precursors	Reaction Conditions	Color	QY (%)	Applications	Reference
B, N Co-Doped CQDs						
Hydrothermal	Branched polyethylenimine and 4-formylphenylboronic acid	8 h at 220 °C	Blue	15.85	Detection of Fe^{3+} ions (LOD of 1.62 μM), and cell imaging (HeLa cell line)	[108]
Hydrothermal	Citric acid anhydrous, ethylenediamine, and three different kinds of borate—i.e., sodium tetraborate, boric acid, and manganese borate	4 h at 160 °C	Blue	29.01, 51.42, and 68.28	Detection of Hg^{2+} ions (LOD of 7.3 nM) and 2,4,6-trinitrophenol (LOD of 0.35 μM), and cell imaging (HUVEC cell line)	[109]
Hydrothermal	2-hydroxyphenylboronic acid and ethylenediamine	12 h at 180 °C	Yellow-green	6.59	Detection of Cr(VI) (LOD of 0.5 μM), anti-counterfeiting and cell imaging (HeLa cell line)	[110]
Hydrothermal	3-aminobenzeneboronic acid and 1,2-ethylenediamine	7 h at 160 °C	Green	47	Determination of α-glucosidase activity and its inhibitors in water samples and living cells	[111]
Hydrothermal	2-aminophenylboronic acid, 3-aminophenylboronic acid monohydrate, or 4-aminophenylboronic acid hydrochloride	8 h at 160 °C	Blue	~7	Detection of p-nitrophenol (LOD of 0.2 μM)	[112,113]
Hydrothermal	3-aminophenylboronic acid	4 h at 180 °C		25.9	Detection of Cr(VI) (LOD of 0.28 μM) and dopamine (LOD of 4.6 μM)	[114]
B, S Co-Doped CQDs						
Hydrothermal	Borax and poly(sodium-p-styrenesulfonate)	8 h at 200 °C	Blue	25.7	Detection of diethylstilbestrol (LOD of 0.06 μM)	[115]
F, N Co-Doped CQDs						
Microwave-assisted carbonation route	Citric acid, urea and sodium fluoride	750 W for 5 min	Yellow	-	In vitro and in vivo cell imaging	[116]
N, P Co-Doped CQDs						
Hydrothermal	Trimesic acid, urea, polyethylene diamine branched, and ortho-phosphoric acid	15 h at 180 °C	Blue	0.41	Label free detection of chromium (II) ions (LOD of 0.1 μM)	[117]
Low-temperature heating	Sucrose, 1,2-ethylenediamine and phosphoric acid	50 min at 80 °C	Blue	12.7	Detection of hemoglobin (LOD of 0.29 nM) in human urine samples and human blood samples, and also in cell imaging (HepG2 cell line)	[118]
Hydrothermal	Pyridoxal 5-phosphate and ethanediamine	4 h at 180 °C	Blue	15.4	Detection of cobalt (Co^{2+}) ions with LOD of 0.053 μM	[119]
Microwave-assisted thermolysis	N-phosphonomethyl aminodiacetic acid and ethylenediamine	700 W for 7 min	Blue	17.5	Cell imaging (HeLa cell line)	[120]

Table 1. *Cont.*

Synthesis Method	Precursors	Reaction Conditions	Color	QY (%)	Applications	Reference
N, P Co-Doped CQDs						
Hydrothermal	Citric acid and diammonium phosphate	1 and 4 h at 180 °C	Blue	59 and 10.58	(i) Detection of Fe^{3+} ions in cancer cells and (ii) detection of iodide (LOD of 0.32 µM) and Fe^{3+} ions (LOD of 72 nM)	[121,122]
Acid-base neutralization spontaneous heat	Glucose, 1,2-ethylenediamine, and concentrated phosphoric acid	-	Green	9.59	Detection of curcumin (LOD of 58 nmol/L) and cell imaging	[123]
Solvothermal	Citric acid, urea, and phosphoric acid in dimethyl formamide solution	24 h at 180 °C	Greenish yellow	15	Detection of Fe^{3+} ions (LOD of 50 nM)	[124]
Hydrothermal	Diethylenetriaminepenta(methylenephosphonic acid) and m-phenylenediamine	5 h at 200 °C	Green	32	Cell imaging (A549 and KB cell line)	[125]
Microwave	m-phenylenediamine, ethylenediamine, and ortho-phosphoric acid	800 W for 40 s	Blue and green	51 and 38	Detection of carbendazim (LOD of 0.002 µM)	[127]
Hydrothermal	Eleocharisdulcis juice	5 h at 90, 120, 150 °C	Navy blue, blue, and cyan	3.3, 11.2 and 8.6	Fluorescent ink for anti-counterfeiting, and detection of Fe^{3+} ions (LOD of 0.56 µM)	[128]
Hydrothermal	Adenosine-5'-triphosphate	2 h at 300 °C	Blue	23.5	Sensing platform for live cell imaging of reactive oxygen species and reactive nitrogen species, including ClO-, ONOO-, and NO in macrophages	[129]
Hydrothermal	Alendronate sodium	20 h at 180 °C	Blue	35	Detection of uranyl ions (LOD of 4.5 nM) in hair and water samples, and also in cell imaging (BT474 cell line)	[130]
N, S Co-Doped CQDs						
Microwave-assisted pyrolysis	Rice and N-acetyl-L-cysteine (NAC)	800 W for 30 min	Blue	2.36	-	[131]
Hydrothermal	Pomegranate juice and L-cysteine	5 h at 120 °C	Blue	4.8	Detection of cephalexin (LOD of 10 µM)	[132]
Combustion	Cellulose-based biowaste of willow catkin soaked in N/S aqueous solution containing urea and sulfuric acid		Blue	13.3	Detection of Fe^{3+} ions (LOD of 0.03 µM) and intracellular imaging (HeLa cell line)	[133]
Microwave	Citric acid, urea, and sodium thiosulfate	700 W for 5 min	-	-	Detection of nitric oxide (LOD of 0.3 µM) in fortified serum solutions	[134]
Hydrothermal	Thiourea, urea, and sodium citrate	6 h at 200 °C	Blue	16	Fluorescence quenching studies in bovine hemoglobin	[135]
Hydrothermal	Garlic	10 h at 180 °C	Blue	13	Detection of Fe^{3+} ions (LOD of 0.32 µM) in lake water and tap water, and in cell imaging (RAW264.7 cell line)	[136]
Hydrothermal	Garlic	3 h at 200 °C	Blue	17.5	Cell imaging (A549 cell line) and free radical scavenging	[137]
Hydrothermal	Garlic and ethylenediamine	6 h at 200 °C	Blue	5.1–20.5	Detection of Fe^{3+} ions (LOD of 0.2 µM)	[138]

Table 1. *Cont.*

Synthesis Method	Precursors	Reaction Conditions	Color	QY (%)	Applications	Reference
		N, S Co-Doped CQDs				
Hydrothermal	Citric acid and cystamine dihydrochloride	6 h at 160 °C	Blue	39.7	Detection for Cr(VI) (LOD of 0.86 μM), and multicolor cell imaging (HeLa cell line)	[139]
Hydrothermal	α-lipoic acid, sodium hydroxide, and ethylenediamine	1, 3, 7, 11, 15 and 19 h at 250 °C	Blue	54.4	Detection of Fe^{3+} ions (LOD of 4 μM), and multicolor cell imaging (HeLa cell line)	[140]
Hydrothermal	Citric acid and thiamine hydrochloride	5 h at 160 °C	Blue	63.8	Detection of Ag^+ ions (LOD of 0.4 μM) and Cys (LOD of 0.35 μM)	[141]
Hydrothermal	Citric acid and l-cysteine	3 h at 200 °C	Violet-Blue	73	Cell imaging (HeLa cell line)	[142]
Microwave	Citric acid and l-cysteine	700 W for 40 secs	Blue	78 ± 10	Detection of bilirubin (LOD of 0.12 nM)	[143]
Solvothermal	Sodium lignosulfonate and p-phenylenediamine	9 h at 200 °C	Green	5.7	Detection of Ag^+ ions (LOD of 11.6 μM) and Fe^{3+} (LOD of 1.7 μM) in real water samples.	[144]
Hydrothermal	m-phenylenediamine and concentrated sulfuric acid	10 h at 200 °C	Yellow	43	White light emitting diode (WLED)	[145]
Hydrothermal	Kappa carrageenan and urea	5 h at 210 °C	Green	69.27	Detection of acetone (LOD of 72 μM) in human fluids (blood and urine)	[146]
Hydrothermal	Allium fistulosum	3 h at 220 °C	Blue	10.48	Multicolor cell imaging in MCF-7 and K562 cell cytoplasm	[147]
Hydrothermal	Enteromorpha prolifera (algae genera for green tide)	3, 6 or 10 h at 180 °C	Blue	12.3	Detection of Fe^{3+} ions (LOD of 0.5 μM)	[148]
Hydrothermal	Glutathione	6 h at 200 °C	Blue	17.5	Detection of tetracycline (LOD of 0.04 μM) and temperature probe	[149]
Hydrothermal	Casein	4 h at 180 °C	Blue	31.8	Detection of Hg^{2+} ions (LOD of 6.5 nM) and biothiols such as l-cysteine (LOD of 23.6 nM), homocysteine (LOD of 12.3 nM) and glutathione (LOD of 16.8 nM)	[150]
Hydrothermal	Feathers, egg white, egg yolk, and manure from pigeon	3 h at 300 °C	Blue	24.87, 17.48, 16.34, and 33.50	Detection of Hg^{2+}/Fe^{3+} ions with LOD of 10.3/60.9 nM	[151]

* LOD—Limit of detection.

2.3.6. B, F, N, P, and/or S Co-Doped CQDs

Liu et al. synthesized B, N, and S co-doped CQDs with QY of 5.44% via hydrothermal reaction (8 h at 180 °C) of 2 and 5 diaminobenzenesulfonic acid, and 4-aminophenylboronic acid hydrochloride [152]. In another similar study, Huang et al. reported the synthesis of B, N, and S co-doped CQDs with blue emission and QY of 8.9%, by using hydrothermal reaction (12 h at 210 °C) of D-(+)-maltose monohydrate, boracic acid, and thiocarbamide, wherein B is used as an electron acceptor dopant which might improve the stability of the CQDs. [153]. Moreover, these co-doped CQDs have shown the stable fluorescence intensity at different pH values (3–12) and temperatures (15–40 °C).

Analogously, Das et al. have used hydrothermal reaction (6 h at 180 °C) of citric acid, thiourea, and 3-amino phenyl boronic acid to prepare B, N, and S co-doped CQDs with multi-color emission and enhanced QY with28% [154]. This fluorescent enhancement is mainly ascribed to (i) the introduction of new kind of surface states that facilitated high yield of radiative recombination, due to N doping, and (ii) the enhancement in the effect of N atoms in co-doped CQDs through a cooperative effect, due to the presence of S.

In another investigation, Chen et al. developed N, P, and S co-doped CQDs via hydrothermal treatment (5 h at 120 °C) of a single precursor—i.e., natural foxtail millet without any extra additives or organic agents (self-doping), where the resultant CQDs have exhibited blue-green luminescence and QY of 21.2%. [155]. Moreover, in virtue of co-doping of the multi-atoms (N, P, and S), the active sites in the CQDs surface might have been effectively passivated by the doping elements due to their strong electron-withdrawing abilities. In addition, the doped heteroatoms might have also contributed to the stabilization of excitons, and further altered the whole electronic structure of these CQDs, which consequently facilitated the enhancement in the recombination yield.

3. Applications

3.1. Electrical/Electronics

3.1.1. Light Emitting Diodes

Electricity can be conserved by using light emitting diodes (LEDs). Nowadays, many researchers have explored the usage of different fluorescent materials including doped/co-doped CQDs for use as LED source. For instance, Khan et al. have recently fabricated an LED by packing a flexible film (based on N-doped CQDs-polyvinyl alcohol (PVA) composite) on the top of a 395 nm n-UV-Chip, which have provided a potentially healthy green light [156]. Herein, N-doped CQDs are initially developed with green emission via solid state reaction (1 h at 200 °C) of ammonium citrate and urea, and then consequently dispersed in PVA matrix for making the composite film. Moreover, (i) the quantum efficiency of the composite film upon excitation at 400 nm is calculated to be 9.5%, and (ii) the electroluminescent (EL) spectrum of fabricated solid-state LED has shown emission spectrum (ranging from 440–800 nm) with intense green emission at 514 nm, where the LED can realize cold light with CIE (Commission Internationale de l'Éclairage) coordinates of (0.2772, 0.4864) as shown in Figure 10. In another very recent study, Zhou et al. have fabricated white LED (WLED) by combining (i) a blue chip (at 465 nm) and (ii) a sturdy yellow-emitting material—by assembling the as-synthesized N and S co-doped CQDs and epoxy resin [145]. It has been revealed that the CIE coordinates of (0.27, 0.29)—for the as-prepared WLED—is close to the pure white light coordinate of (0.33, 0.33).
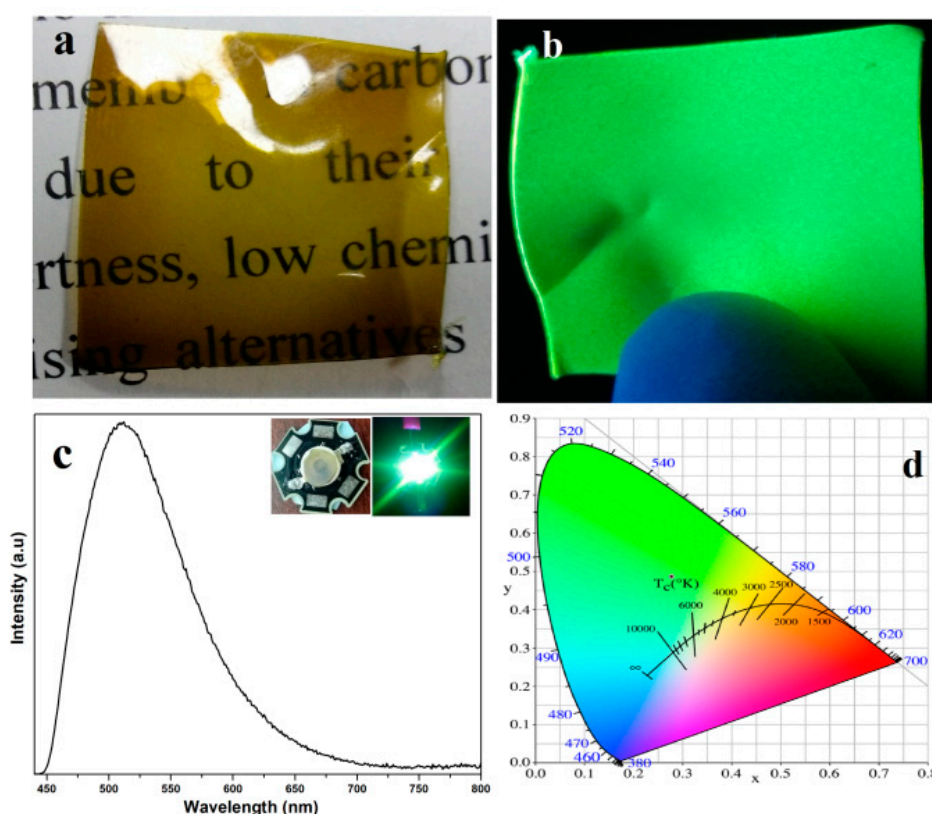
Figure 10. N-doped CQDs- polyvinyl alcohol (PVA) composite under (**a**) daylight and (**b**) under 365 nm UV irradiation. (**c**) EL emission spectra of solid state light emitting diodes (LED) upon 395 nm excitation: (inset) solid-state LED of N-doped CQDs-PVA composite under daylight (left) and under 395 nm UV-chip in (right); (**d**) Commission Internationale de l'Éclairage(CIE) coordinate of green LED. Reproduced with permission from Khan et al. [156] Copyright ACS, 2018.

3.1.2. Solar Cells

Solar cells are widely employed in the production of electricity to meet the growing global demand for energy, and utilized as an alternate to the conventional sources, for instance coal. The solar cells are usually fabricated with materials including perovskites, kesterites, up-/down- conversion based rare earth elements (e.g., lanthanide) doped, dye-sensitized, organic semiconductors including polymers, and QDs made of cadmium sulphide (CdS), cadmium selenide (CdSe), lead sulphide (PbS), and so on. Nonetheless, doped/co-doped CQDs have been recently used in the conversion of solar energy into electrical energy (via solar cells) due to their high photostability in comparison to the semiconductor QDs [157]. For instance, Zhang et al. have applied the N-doped CQDs as metal-free sensitizers in dye-sensitized solar cells (DSSCs), where the CQDs-sensitized titanium oxide (TiO_2) electrodes are prepared via hydrothermal reaction (4 h at 100 °C) between TiO_2 electrode and N-doped CQDs in aqueous solution [158]. Herein, the preliminary study has shown that the short circuit current (Jsc), the open circuit voltage (Voc) and fill factor (FF) values from current density–voltage (J–V) measurements have, respectively, reached 0.69 mA cm^{-2}, 0.46 V, and 43% (under one sun illumination (AM 1.5) and irradiation intensity of 100 mW cm^{-2}), achieving a power conversion efficiency (PCE) of 0.13% for N-doped CQDs-TiO_2 based DSSCs device. Similarly, Wang et al. have fabricated solar cells (DSSC) by sandwiching gel electrolytes between a TiO_2 electrode sensitized N-doped CQDs and a platinum (Pt) counter electrode (which are split by a 25-mm-thick hot-melt ring and sealed by heating), where the CQDs are made via pyrolysis (3 h at 200 °C) of citric acid and urea [159]. Herein, the results have shown that the DSSC has Jsc, Voc, FF, and PCE of 2.65 mA cm^{-2}, 0.47 V, 62.5%, and 0.79%, respectively.

Moreover, the incident photon-to-electron conversion efficiency (IPCE) value is over 10% between 400 and 550 nm, and the highest value of IPCE even approaches 34% for N-doped CQDs.

In another investigation, Mariotti et al. primarily fabricated the solar cell device (DSSC), whose structure consists of (i) the transparent conducting oxide indium tin oxide (ITO, 150 nm), (ii) a TiO_2 hole blocking layer (40 nm), (ii) N-doped CQDs (prepared via atmospheric pressure microplasma in contact with water containing C (citric acid) and N (ethylenediamine) sources) spray-coated from solution as the active layer, and (ii) gold (Au) contacts (340 nm)—sputtered directly on top of the CQD layer, as shown in Figure 11 [160]. The device have displayed good rectification with Jsc, Voc, high FF, and PCE of 0.23 mA cm^{-2}, 1.8 V, 79%, and 0.8%, respectively, in the J-V curve of DSSC under one full sun illumination (AM 1.5 G). Analogously, Zhao et al. have presented experimental realization of co-sensitization of N-doped CQDs with N719 dye for solar cells [161]. A maximized PCE of 9.29% under one sun illumination (AM 1.5 with irradiation intensity of 100 mW cm^{-2}) is achieved for N_{300}-CQDs/N719 co-sensitized solar cells in comparison with 8.09% for N_{300}-CQDs-free device (ascribed to up-conversion and hole extraction behaviors of CQDs), where N_{300}-CQDs are prepared via hydrothermal reaction of 200-mesh strawberry powders and $NH_3.H_2O$ (300 mL). In addition, the values of Jsc, Voc and FF are correspondingly determined to be 18.6 mA cm^{-2}, 0.736 V and 67.9%. In another similar study, Yang et al. have fabricated N-doped CQDs based solar cells that yielded the maximized solar-to-electrical conversion efficiency of 0.17% with FF of 67%, where the N-doped CQDs are prepared via optimized hydrothermal reaction of a natural source—i.e., Eichhornia crassipes (self-doping) [162].
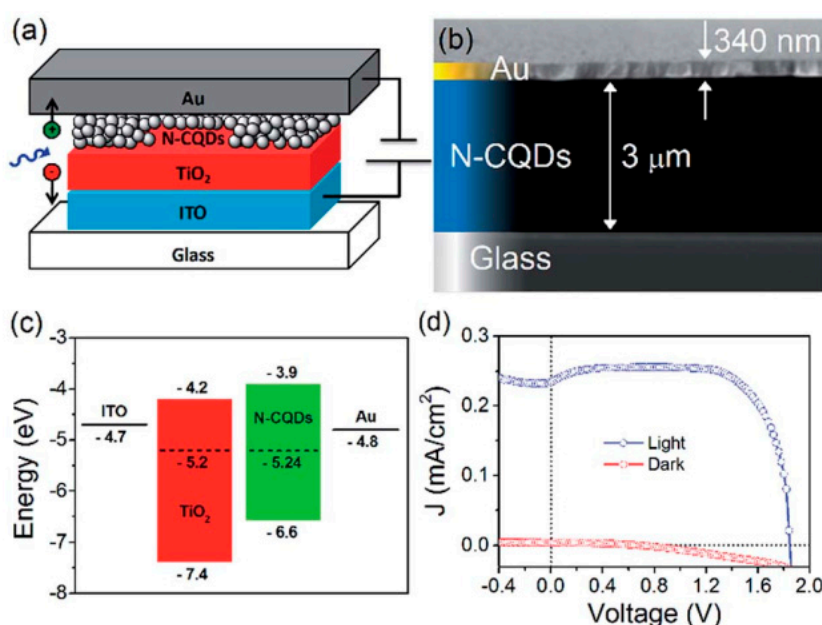

Figure 11. (**a**) N-doped CQDs based solar cell device structure, (**b**) cross-sectional scanning electron microscopy imaging (X-SEM) of the device, (**c**) energy band structure of the fabricated devices and (**d**) current density–voltage (J–V) curve for the best device. Reproduced with permission from Mariotti et al. [160] Copyright RSC, 2017.

Nevertheless, Chandra et al. utilized S-doped CQDs for solar cell application, wherein the device was fabricated by (i) initially making a solution mixture of phenyl-C60-butyric acid methyl ester (PCBM) and S-doped CQDs (at weight ratio of 1:3) via sonication, and (ii) deposition of the solution mixture on the pre-cleaned ITO coated glass substrate through spin coating inside a glove box under a nitrogen (N_2) atmosphere [99]. The device has shown a Jsc, Voc, FF, and PCE of 3.19 mA cm^{-2}, 617 mV, 37%, and 0.73%, respectively, in the J-V curve under white light illumination with incident intensity of 100 mW cm^{-2}. Moreover, the authors have concluded that the cell fabricated by the deposition of

CQDs-PCBM has showed enhanced Voc and FF, which might be ascribed to the S atoms present on the surface of the CQDs.

In another recent investigation, Wang et al. have prepared N and S co-doped CQDs based organic solar cell with configuration of ITO/ZnO (or ZnO:N-doped CQDs or ZnO:N and S co-doped CQDs)/PTB7-Th:PC71BM/MoO3/Al—as shown in Figure 12 [163]. Herein, ZnO is zinc oxide, PTB7 This poly[4,8-bis(5-(2-ethylhexyl)thiophen-2-yl)benzo[1,2-b:4,5-b']dithiophene-co-3-fluorothieno[3,4-b]thiop hene-2-carboxylate], PC71BM is [6,6]-phenyl-C71-butyric acid methyl ester, MoO$_3$ is molybdenum oxide and Al is aluminium. The results have shown that, as compared to others, the ZnO:N and S co-doped CQDs based device have exhibited better Jsc, Voc, FF, and PCE of 17.2 mA cm^{-2}, 0.80 V, 0.68, and 9.36%, respectively (without S-shaped kink), in the J-V curve under simulated AM 1.5G sun light with incident intensity of 100 mW cm^{-2}. The performance improvement and the elimination of light soaking effect for ZnO:N and S co-doped CQDs cells are attributed to the ZnO surface defect passivation by N and S co-doped CQDs (as in Figure 12), as confirmed via the fluorescence spectroscopy and Scanning Kelvin probe microscopy.
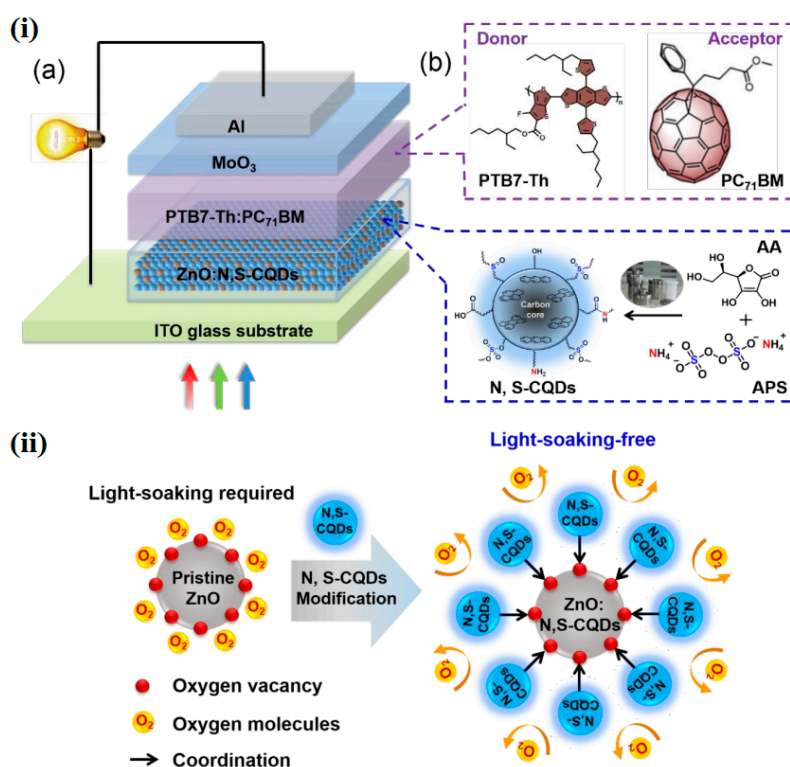

Figure 12. (i) (**a**) Device configuration of inverted organic solar cells (OSCs) and (**b**) structural formula of active layer materials and sketch map of the synthesis of N and S co-doped CQDs, and (ii) proposed surface defects passivation mechanism of N and S co-doped CQDs on ZnO nanoparticles. Reproduced with permission from Wang et al. [163] Copyright ACS, 2019.

3.2. Fluorescent Ink for Anti-Counterfeiting

Guo et al. found that B and N co-doped CQDs could be used as fluorescent ink for writing letters/numbers/Chinese characters on Xuan Paper and weighing paper for anti-counterfeiting—as shown in Figure 13 [110]. These letters/number/characters have gradually changed from light yellow to colorless (under visible light) with the decrease in the concentration of the CQDs. However, they have been observed with blue color upon the irradiation of UV light with wavelength of 365 nm, which retained for 3 months, revealing their potentiality for invisible fluorescent ink for anti-counterfeiting. For this purpose, B and N co-doped CQDs are mixed with PVA solution to fabricate CQDs/PVA film, which exhibited (i) light yellow under visible light, and (ii) blue emission in 365 nm UV light.
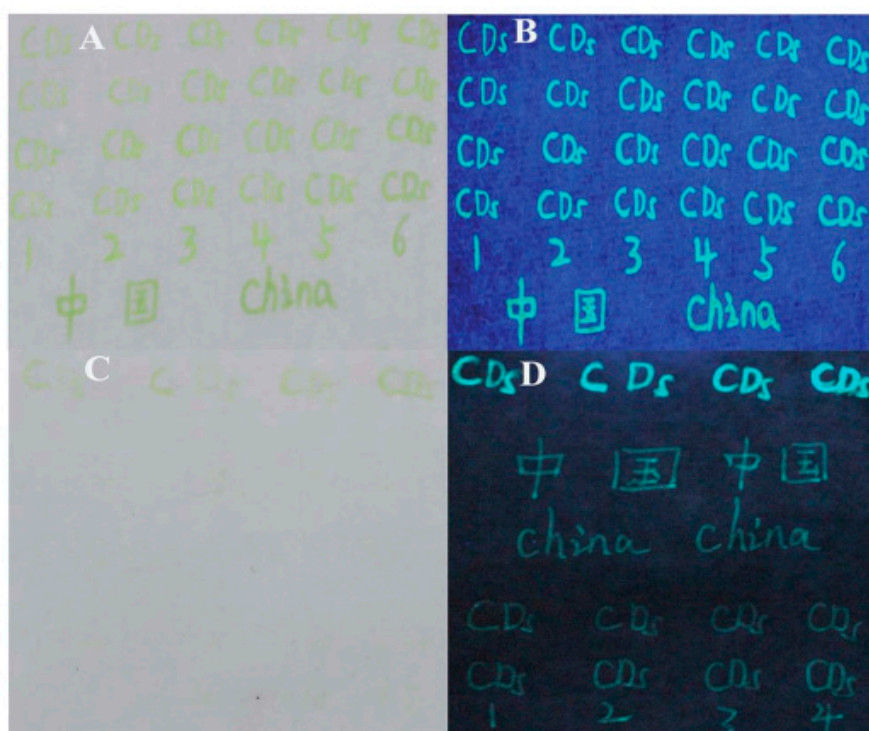
Figure 13. Handwritten letters, number and Chinese characters using B and N co-doped CQDs as ink on Xuan paper (**A**,**B**) and weighing paper (**C**,**D**) under visible light (**A**,**C**) and 365 nm UV light (**B**,**D**). Reproduced with permission from Guo et al. [110] Copyright RSC, 2017.

Similar to the above study, Bandi et al. have also explored the potentiality of N and S co-doped CQDs for fluorescent ink for use in anti-counterfeiting [164]. For this purpose, the following steps are followed: a sketch pen is initially filled with N and S co-doped CQDs based aqueous solution and is used for writing some text (for instance "Osmania University") on commercial filter paper, and then the filter paper is viewed under visible and UV light. Herein, the text has appeared as blank under visible light; however, it is clearly visible by showing blue fluorescence under UV light (as shown in Figure 14), which is reproducible even after 30 days (when stored under ambient conditions). In addition, these N and S co-doped CQDs are safely utilized as ink pads to form human fingerprints that do not contaminate the fingers, as shown in Figure 14. Similar studies were performed by Bao et al. [128], Liu et al. [165], and Fan et al. [166].
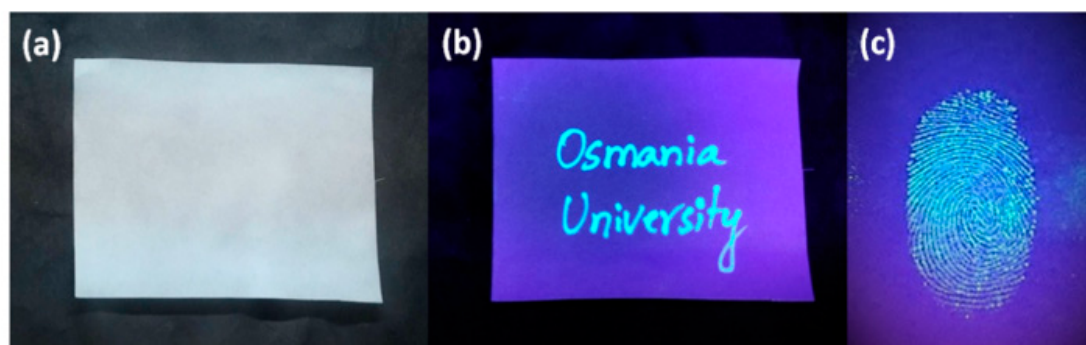

Figure 14. Information loaded on commercial filter paper using N and S co-doped CQDs invisible ink under (**a**) daylight and (**b**) 365 nm UV light. (**c**) N and S co-doped CQDs formed fingerprints under 365 nm UV light. Reproduced with permission from Bandi et al. [164] Copyright ACS, 2018.

3.3. Optical Sensors

Doped/co-doped CQDs do possess special abilities to optically sense (based on color change/quenching process) different targets including metal ions (mainly Fe^{3+} and Hg^{2+} ions), chemical/biological molecules (including ascorbic acid, hydrogen peroxide), and pesticides Commonly, there are four major types of fluorescence response modes for optical sensing: (i) fluorescence "off", (ii) fluorescence "on", (iii) fluorescence resonance energy transfer—FRET, and (iv) ratiometric response [31]. Nevertheless, CQDs mainly utilize fluorescence "off"/"on" mechanism for easy detection of the targets.

3.3.1. Sensing of Metal Ions

Iron (Fe^{3+}) Ions

Iron (Fe^{3+}) ions are biologically important since they (i) are significant co-factors in numerous regulatory proteins, and (ii) play important roles in oxygen uptake/metabolism and electron transfer [31]. Nevertheless, overloading or deficiency of these Fe^{3+} ions in biological systems might create a variety of disorders. Hence, there is a need for sensitive detection of these Fe^{3+} ions, which was recently done in an effective manner based on the fluorescence process by using the as-developed doped/co-doped CQDs. For example, Jana et al. prepared B-doped CQDs and used them to detect Fe^{3+} ions down to 3.1 nM level (based on the quenching process), which is much lower than the permissible limit of these ions in water (i.e., 0.3 mg/L or ~5.357 μM), as suggested by World Health Organization (WHO) [63].

In another investigation by Lv et al., applied N-doped CQDs in the detection of Fe^{3+} ions among other metal ions including Na^+, K^+, Mg^{2+}, Co^{2+}, Ca^{2+}, Ni^{2+}, Cu^{2+}, Cd^{2+}, Li^+, Pb^{2+}, Fe^{2+}, Al^{3+}, Cr^{3+}, Ag^+, Mn^{2+}, Sn^{2+}, and Zn^{2+} [75]. Herein, the spectroscopic data have revealed that these CQDs have exhibited (i) a sensitive response to Fe^{3+} ions in the range of 0.5–1000 μM with limit of detection (LOD) of 0.079 μM and (ii) good response as a fluorescence sensor in real environmental samples. Similarly, Wu et al. have developed N-doped CQDs and investigated the relationship between the concentration of Fe^{3+} ions and the fluorescent quenching factors $\{(F_0-F)/F_0\}$ in the range of 0–150mM, where F_0 and F indicate the fluorescence intensities of these CQDs at 460 nm in the absence and presence of Fe^{3+} ions, respectively [76]. It has been noted that the quenching factors are in a linear relationship with Fe^{3+} ions concentration in the range of 0–20 μM, and the LOD is figured out as 3.7 μM.

In another study, Li et al. detected Fe^{3+} ions by using N-doped CQDs, where a good linear correlation is attained between the fluorescence intensities and the concentration range of 0–100μM, with LOD of 0.001 M [82]. Similarly, Wu et al. utilized N-doped CQDs as a fluorescent probe for Fe^{3+} detection via fluorescent quenching, where high selectivity and sensitivity are achieved with LOD of Fe^{3+} as low as 0.21 nM in the acidic environment [85]. In a similar investigation, Hou et al. applied the as-prepared N-doped CQDs to the 'on-off-on' fluorescence sensing platform with the step-wise addition of Fe^{3+} ions, where the LOD is calculated to be 50 nmol/L based on quenching phenomenon, which could be ascribed to the changes in the surface electron-hole recombination annihilation due to the formation of Fe^{3+}-complexes on the surface of the CQDs [86]. Moreover, Xu et al. have shown that the fluorescence of S-doped CQDs is effectively and selectively quenched by Fe^{3+} ions in the range of 1–500 μM as compared to other ions including Zn^{2+}, Ni^{2+}, Fe^{3+}, K^+, Mn^{2+}, Mg^{2+}, Cd^{2+}, Ca^{2+}, Cu^{2+}, and Ba^{2+} ions, displaying the ability of these CQDs to probe Fe^{3+} ions with LOD of 0.1 μM [101]. Naik et al. used S-doped CQDs to detect Fe^{3+} ions but with dual method, where the linear detection range of these CQDs towards these Fe^{3+} ions is in the range of (i) 0–872 μM with LOD of 0.56 μM fluorometrically, and (ii) 0–290 μM with LOD of 32.30 nM via UV-Vis spectrophotometrically [106]. In another investigation, Wu et al. proved that the as-prepared S-doped CQDs can be used as an effective fluorescent probe for detection of Fe^{3+} ions sensitively and selectively, with LOD of 177 nM [107].

Analogously, Chandra et al. prepared N and P co-doped CQDs, where their surface have possessed numerous hydroxyl based surface functional groups, which was used in the detection of Fe^{3+} ions in the range of 20–200 μM [121]. Herein, the functional groups might have been induced a preferable formation of metal hydroxide complex on the surface of CQDs during the treatment of Fe^{3+} ions, which

might have consequently decreased the luminescence of the CQDs. This phenomenon was ascribed to Fe^{3+} ions ability to quench the fluorescence of CQDs apparently via electron or energy transfer and preferably chelating with the surface of CQDs. In addition, same authors synthesized N and P co-doped CQDs that are used for the selective detection of Fe^{3+} ions, where the sensing assay of these ions shows a detection range from 0.2–30 µM with a LOD of 72 nM [122]. Moreover, the Fe^{3+} ions are effectively detected in the cancerous cells—MCF-7 and HeLa cells by using N and P co-doped CQDs. In another investigation, Omer et al. showed that N and P co-doped CQDs to be viable fluorescent probes for Fe^{3+} ions determination with high selectivity and sensitivity, where the sensing assay has displayed a linear response in the range of 0.1–0.9 µM Fe^{3+} ions concentration with LOD of 50 nM [124]. Similarly, Li et al. and Bao et al. showed that the fluorescence of N and P-doped CQDs is effectively quenched by Fe^{3+} ions in the linear range of 0.09–60µM with LOD of 0.09 µM, and 5–350µM with LOD of 0.56 µM, respectively [125,128]. In a similar investigation, Chen et al. have developed Fe^{3+} ions based sensor using prepared N and S co-doped CQDs and utilized it to detect Fe^{3+} in environmental waters and also inside the cells (i.e., RAW264.7) with enhanced sensitivity and repeatability, where the linear response is in the range of 2 nM–3 µM with LOD of 0.22 nM [136]. In analogous fashion, Sun et al. proved that quenching the fluorescence of the N and S co-doped CQDs in the presence of Fe^{3+} ions has made them as a luminescent probe for selective detection of Fe^{3+} ions with concentration range of 0–500 µM and LOD of 0.2 µM [138]. In another case, N and S co-doped CQDs were used by Ding et al. and Zhu et al. in determining Fe^{3+} ions within concentration range of 25–500 µM with LOD of 4 µM, and 0.1–0.1 µM with LOD of 4 µM, respectively [140,144]. Similar studies are performed by Xu et al. [148], Zhao et al. [149], and Ye et al. [151].

Liu et al. have developed a colorimetric and fluorescent nanosensor based on B, N, and S co-doped CQDs that helped in a sensitive assay of Fe^{3+} ions in the range of 0.3–546 µM with LOD of 90 nM (by quenching the red emission fluorescence), in comparison to the experiments to determine the potential interfering substances coexisted in urine and serum samples, including various metal cations (Co^{2+}, Hg^{2+}, Mn^{2+}, Zn^{2+}, Al^{3+}, Ni^{2+}, Cu^{2+}, and Fe^{2+}), amino acids (Thr, Try, L-Tyr, Lys, Arg, Glu, Gly, L-Cys, Ala) and glutathione (GSH) [152]. Moreover, Fe^{3+} ions are visualized via this nanosensor through evident color changes of the solution (from red to blue) under sunlight without the aid of UV lamp—as shown in Figure 15.
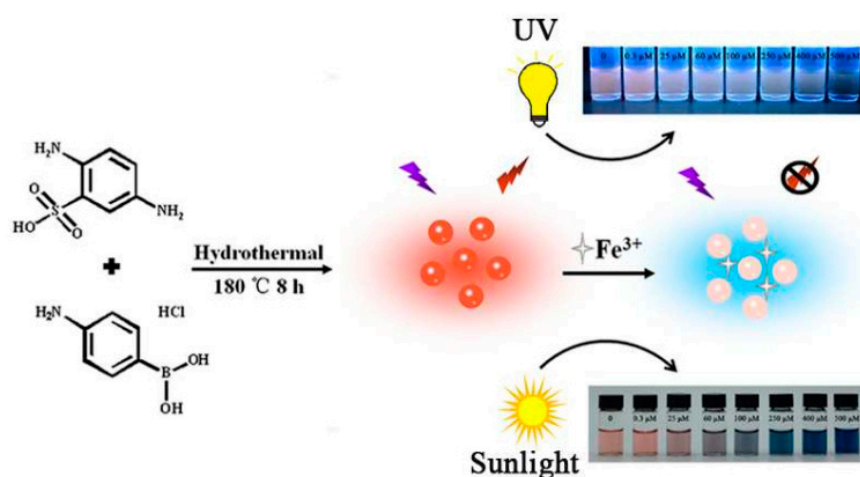

Figure 15. Sensing performance of B, N, and S co-doped CQDs for the detection of Fe^{3+} ions in colorimetric and fluorescent manner. Reproduced with permission from Liu et al. [152] Copyright ACS, 2017.

Mercury (Hg^{2+}) Ions

It is extremely necessary to sense mercury (Hg^{2+}) ions to inhibit their hazardous effects in the health of humans and also to the environment. Recently, CQDs (especially doped/co-doped) are

useful in detecting these Hg^{2+} ions sensitively and selectively in different conditions. For instance, Zhang et al. have prepared blue-emitting N-doped CQDs (with QY of 15.7%) by using folic acid as both C and N sources via hydrothermal process (12 h at 180 °C), which have served as an efficient platform for label-free sensitive detection of Hg^{2+} ions with LOD of 0.23 μM [167]. Moreover, these CQDs based Hg^{2+} ions sensor has been successfully utilized in the Hg^{2+} analysis in tap water and real lake water samples. Analogously, Huang et al. prepared N-doped CQDs (with QY of 42.2%)by using the reaction between tartaric acid, citric acid, and ethylenediamine (as the precursors) in oleic acid media via solvothermal process (0.5 h at 220 °C)to evaluate their ability as fluorescent probe for "off-on" detection of Hg^{2+} ions [168]. Initially, these CQDs (with a concentration of 2.1 μg/mL)were added to the solution containing various metal ions including Cr^{6+}, Cu^{2+}, Ni^{2+}, Co^{2+}, Cd^{2+}, Zn^{2+}, Mg^{2+}, Sr^{2+}, Pb^{2+}, Ba^{2+}, Al^{3+}, K^+, Na^+, Fe^{2+}, and Hg^{2+} to form a final concentration of 100 μM, and their fluorescence spectra are consequently recorded under an excitation wavelength of 360 nm. It was noted that the fluorescence intensity has predominantly decreased with the addition of Hg^{2+} ions (with LOD of 83.5 nM) as compared to other ions, which indicates that the N-doped CQDs are highly selective towards these Hg^{2+} ions. Similarly, Feng et al. used hydrothermal treatment (12 h at 180 °C) of strawberry juice to prepare N-doped CQDs (with nitrogen content and QY of 6.88% and 6.3%) that has been used to detect Hg^{2+} ions with a linear range from 10–50 μM and LOD of 3 nM [169]. In another study, Tang et al. effectively used N-doped CQDs (synthesized using microreactor with foamy copper) as nanoprobes for Hg^{2+} ions detection with LOD of 2.104 nM [88].

Moreover, Xu et al. optimized the molar ratios of the precursors—sodium citrate and diammonium phosphate (15:1, 19:1, 24:1, and 28:1), the reaction temperatures (140, 150, 160, 170, 200, and 220 °C), and reaction time periods (2, 4, 6, 8, and 10 h) in hydrothermal method to effectively synthesize N and P co-doped CQDs (with enhanced QY of 53.8%) for detection of Hg^{2+} ions at an excitation wavelength of 440 nm [170]. Herein, the resultant calibration curve for Hg^{2+} ions has exhibited a good linearity in a specific concentration range with LOD and time of 1 nM and 0.5 min, respectively. Moreover, they proposed that there is an indirect evidence for the detection limit advantage with P doping, when compared to previous reports. Analogously, Chandra et al. also synthesized blue emitting N and S co-doped CQDs—with QY of 17.59% via hydrothermal method (4 h at 180 °C) by optimizing the molar ratio (1:0.5, 1:1, 1:1.5, and 1:2) of the N and S precursors—i.e., diethylenetriamine and thiomalic acid, respectively—for the effective detection of Hg^{2+} ions [171]. Herein, the Hg^{2+} ions present in river water and tap water were successfully sensed with LODs of 51.25 nM and 52.45 nM, respectively. Moreover, the as-prepared CQDs have efficiently used in the intercellular Hg^{2+} ions detection in triple negative breast cancer cells based on fluorescence quenching. In another investigation, Wang et al. synthesized blue emitting N and S co-doped CQDs (with QY of 17.6%)by using citric acid and rubeanic acid (i.e., dithiooxamide) as C and N/S precursors through microwave-assisted hydrothermal process (800 W for 2.5 min) and directly using them as a sensor for mercury(II)/Hg^{2+} ions [172]. It has been noted that the fluorescence of these CQDs is almost quenched after adding 20 μM Hg^{2+}, where the LOD is calculated to be 0.18 μM. In addition, these authors have developed CQDs-based test paper for rapidly and independently sensing the Hg^{2+} ions in real water samples (without any spectrometers or other large equipment), where the emission of this test paper has become dim, once it is immersed in Hg^{2+}-spiked river-water without buffering for even 1 s.

Chromium (Cr) Ions

Chromium (VI) [Cr(VI)] and Cr(II) ions are hazardous to human health, in comparison to other valence states including Cr(0) and Cr(III), because of their greater mobility and carcinogenic properties. Hence, determination of these chromium ions in environmental samples is important, and its concentration in drinking water should be strictly regulated to a lower micromolar level. Recently, doped/co-doped CQDs have been shown to be useful in determining these Cr(VI) or Cr(II) ions effectively. For example, Zheng et al. fabricated an "On"−"Off" fluorescent probe based N-doped

CQDs for the detection of Cr(VI) based on the inner filter effect (IFE), since the absorption bands of Cr(IV) has completely covered the emission and excitation bands of these CQDs [89].

In another study, Guo et al. have identified that the B and N co-doped CQDs can be utilized to sense $Cr_2O_7^{2-}$ (dichromate) ions in aqueous solution due to the $Cr_2O_7^{2-}$ induced fluorescence quenching [110]. In the CQDs based sensing system, as low as 0.5 mM (i.e., LOD) of $Cr_2O_7^{2-}$ is detected and a good linear relationship is obtained in the range of 0–250 mM. Analogously, Singh et al. synthesized N and P co-doped CQDs (that exhibited bright blue color under UV-light with CIE coordinate (0.20, 0.22) along with high QY of 73%), and they have acted as an "On"-"Off" fluorescent nanoprobe for selective/sensitive detection of Cr (VI) below the permissible limit via IFE and static quenching mechanism [173]. Moreover, the Cr (VI) has been reduced to lower valent chromium species. Similarly, Omer et al. prepared N and P co-doped CQDs that showed high selectivity towards the chromium (II) ions, and the fluorescence intensity quenched by or Cr(II) ions in a linear manner for the concentration range of 0.5–1.3 µM and LOD of 0.1 µM [117]. In a recent investigation, Chen et al. prepared N and S co-doped CQDs whose fluorescence is quenched based on IFE upon Cr(VI) ions addition, resulting in good selectivity and sensitivity towards Cr(VI) [139]. Moreover, the detection for Cr(VI) ions has exhibited a good linear correlation ranging from 1–80 µM with LOD of 0.86 µM.

Molecular Logic Gates

Molecules usually respond to changes in their environment. Moreover, the presence of various ions/neutral-species/pH/temperature/viscosity result in changes in color or emission as a result of the complex interplay of many excited state processes and environmental parameters [174]. A molecular logic gate is mainly defined as a molecule which can perform a logical operation based on one or more physical or chemical inputs and a single output. Moreover, in IMPLICATION logic gate operations, the output is "0" only when input 1 is equal to "1", and the input 2 has to be equal to "0". Otherwise, the rest output is "1". Recently, doped CQDs have gained more attraction for use as molecular logic gates based on their effective fluorescence responses. For instance, Liao et al. have designed N-doped CQDs based IMPLICATION logic gate, which is constructed on Boolean operations when Hg^{2+} ions and biothiol as inputs, whose presence is considered to be the "1" state and their absence as "0" as per the truth table [175]. Herein, N-doped CQDs are prepared via hydrothermal reaction (6 h at 160 °C) of citric acid and ethanol amine.

In analogous fashion, Song et al. have synthesized N and S co-doped CQDs (via hydrothermal treatment (2.5 h at 220 °C) of formamidine sulfinic acid and ethylene glycol) for application in logic gates (for instance, IMPLICATION) operation at 11 pH (as shown in Figure 16), attributed to their excellent "On-Off-On" signal response [176]. These logic gates deploy metal ions and chelators as inputs 1 and 2, and the fluorescence intensity of co-doped CQDs as the optical output. For inputs, the presence of inputs of metal ions (Ag^+, Hg^{2+} or Ni^{2+}) or the respective chelators (ammonium thioglycolate, ethylenediamine, and glycine) is defined as "1″ and the absence of inputs is defined as "0″. For the output, high fluorescence intensity is defined as output "1″ and low fluorescence intensity as output "0″. Moreover, without input or with chelators alone as input, the fluorescence intensity of N and S co-doped CQDs is very high, the output is "1″. With metal ions alone as input, metal ions can efficiently quench the fluorescence of N and S co-doped CQDs, providing an output signal of "0″. When the system is subjected to the two inputs together, the strong interaction between metal ions and chelators releases metal ions from the surface of N and S co-doped CQDs and the output signal is "1″. In another similar study, Bandi et al. converted toxic cigarette butts into N and S co-doped CQDs (with QY of 26%) in the presence of sulphuric acid via hydrothermal approach, for further construction of an IMPLICATION logic gate [164]. Herein, cigarette butts were chosen as precursors, since they are mainly composed of cellulose acetate fibers, and also contain minor amounts of chemicals including polycyclic aromatic hydrocarbons, nicotine, aromatic amines, N-nitrosamine, and tarlike components that are trapped during smoking. The fluorescence switching behavior of these co-doped CQDs in the presence of iron (Fe^{3+}) ions and ascorbic acid has been employed as multiple

molecular logic gates, performing the Boolean algebraic logic operations. The simple single input molecular logic gate NOT has been constructed using Fe^{3+} as single input signal, and the multiple input logic gate IMPLICATION has been ascertained by taking Fe^{3+} and ascorbic acid as input 1 and input 2, respectively. The presence of Fe^{3+} or ascorbic acid has been taken as 1 and their absence as 0. For output, the maximum fluorescence has been taken as 1 and the corresponding quenched fluorescence as 0. The results have showed that only in the presence of Fe^{3+} and absence of ascorbic acid, i.e., input (1, 0), significant fluorescent quenching has been observed and provided output as 0, while in the case of other inputs (0/0, 0/1, 1/1), the output remains 1. The logic symbol, truth table, and output fluorescence intensity at 430 nm are shown in Figure 17.
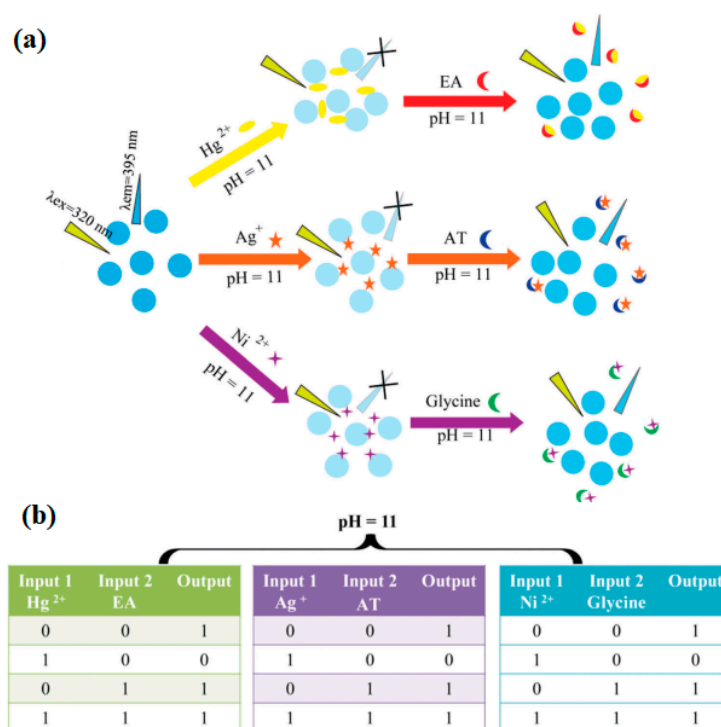

Input 1 Hg^{2+}	Input 2 EA	Output
0	0	1
1	0	0
0	1	1
1	1	1

Input 1 Ag^+	Input 2 AT	Output
0	0	1
1	0	0
0	1	1
1	1	1

Input 1 Ni^{2+}	Input 2 Glycine	Output
0	0	1
1	0	0
0	1	1
1	1	1

Figure 16. (**a**) Illustration of the logic gate operation based on N and S co-doped CQDs, and (**b**) truth table for the logic gate operation. Reproduced with permission from Song et al. [176] Copyright RSC, 2018.

Similarly, Sharma et al. systematically investigated the use of N and S co-doped CQDs (synthesized hydrothermal treatment (5 h at 180 °C) of rose petals—self-doping) for (i) fluorescence "Off-On-Off" response towards sulphide (S^{2-}) and gold (Au^{3+}) ions, whose LOD is determined to be 92.4 nM and 63.1 nM, respectively, and (ii) construction of logic gates which simulate single input logic "YES" and multi-input "INHIBIT" logic system—as shown in Figure 18 [177]. Herein, only in the presence of S^{2-} ions and absence of Au^{3+} ions i.e., input (1, 0), the system generates a marked enhancement in fluorescence and provide output as "1", while in case of other input signals (0/0, 0/1, 1/1), the output remains "0".
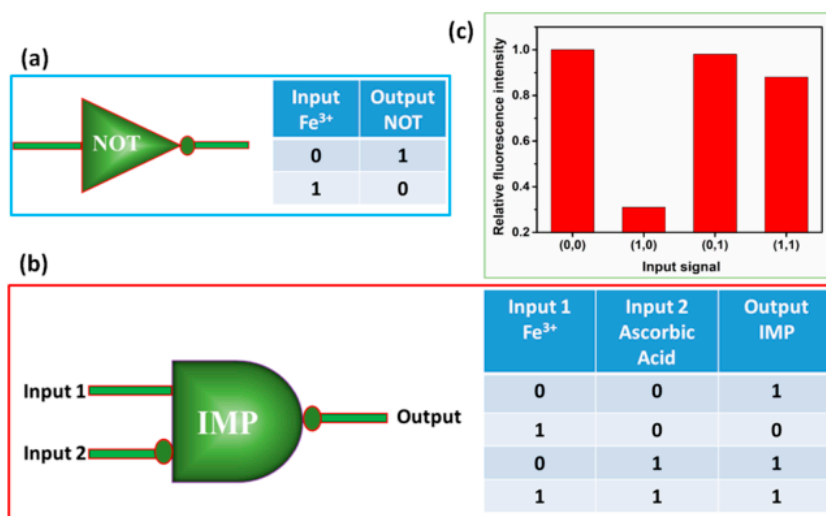
Figure 17. Logic operations using N and S co-doped CQDs: (**a**) logic symbol and truth table of NOT logic gate; (**b**) logic symbol and truth table of IMPLICATION logic gate; and (**c**) fluorescence response of N and S co-doped CQDs under different inputs. Reproduced with permission from Bandi et al. [164] Copyright ACS, 2018.
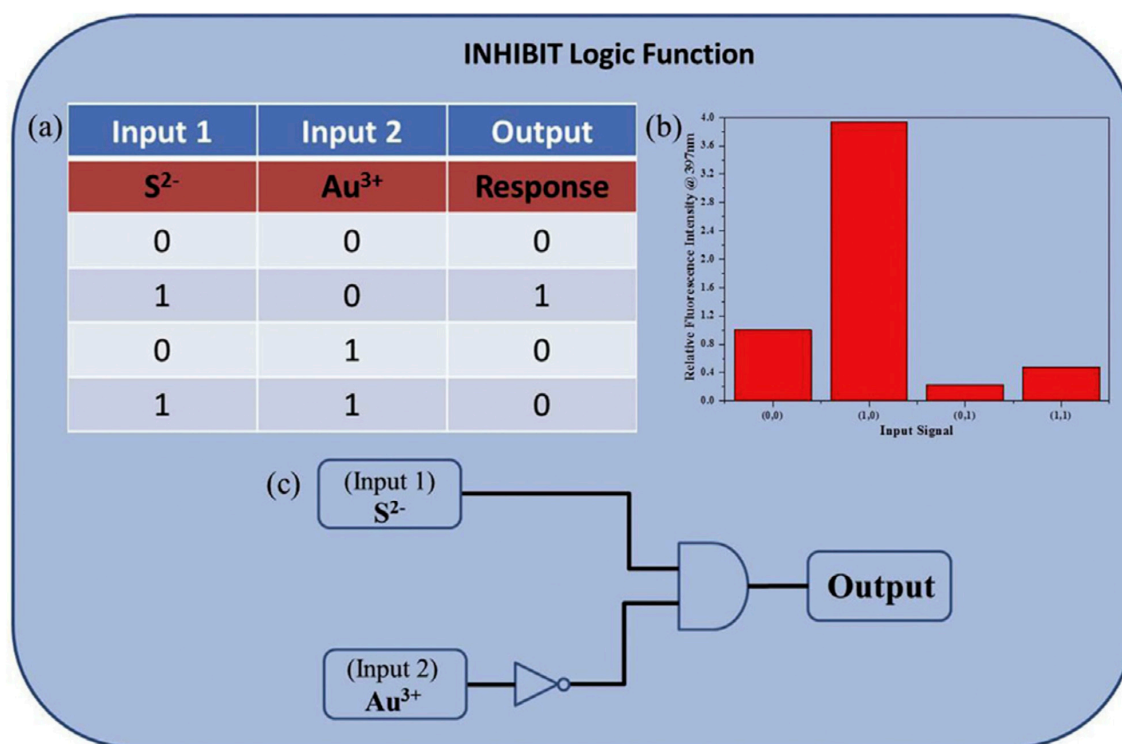

Figure 18. "INHIBIT" logic function using N and S co-doped CQDs. (**a**) Truth table (**b**) Fluorescence response of N and S co-doped CQDs under different inputs (**c**) Symbol of INHIBIT logic. Reproduced with permission from Sharma et al. [177] Copyright Elsevier, 2018.

3.3.2. Detection of Drugs

It is highly important to monitor the levels of drugs (e.g., anti-cancer drugs) in patients in clinics/pharmaceutics continuously to minimize adverse effects, immoderate administration, and/or therapeutic oversights caused by erroneous intake schedules. In recent days, doped/co-doped CQDs are effectively used for drug detection to ensure proper therapy.

Methotrexate

Wang et al. prepared blue emitting N and S co-doped CQDs with QY of 21.6% via hydrothermal reaction (2 h at 200 °C) of ammonium persulfate, ethylenediamine, and glucose for the detection of an anti-cancer drug—methotrexate [178]. Herein, the fluorescence of these co-doped CQDs is significantly quenched by methotrexate via fluorescence resonance energy transfer (FRET) between CQDs and methotrexate—as shown in Figure 19, which is further utilized for high selective/sensitive detection of methotrexate with a linear range up to 50.0 μM and LOD of 0.33 nM. Moreover, this method is also explored for the practical detection of methotrexate in human serum. Similarly, Zhao et al. have fabricated a fluorescence sensor based on IFE of N and S co-doped CQDs for detection of methotrexate at pH of 4, resulting in sensing of the drug at a concentration between 0.4 and 41.3μg/mL with LOD of 12 ng/mL [179]. Herein, these co-doped CQDs (with blue emission and QY of 57.2%) are prepared via hydrothermal reaction (3 h at 200 °C) of citric acid monohydrate and L-cysteine.
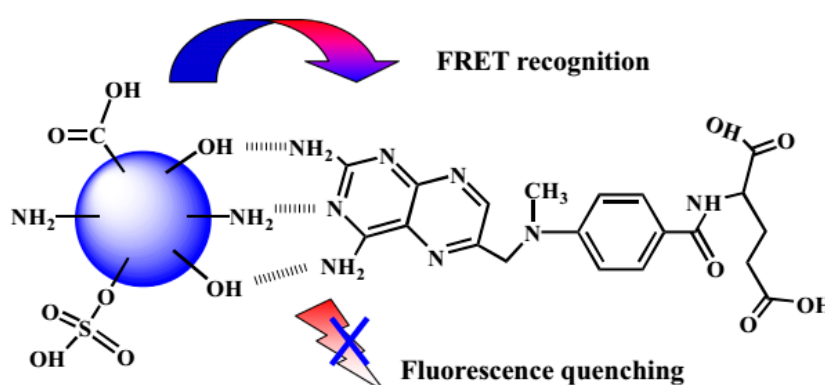

Figure 19. Schematic illustration of the quenching mechanism of N and S co-doped CQDs for detection of methotrexate. Reproduced with permission from Wang et al. [178] Copyright Elsevier, 2015.

Curcumin

Liu et al. prepared N and P co-doped CQDs and utilized as a label-free sensor for determination of curcumin, where the sensor was applied for detection of curcumin in aqueous solution sensitively, while achieving a linear range of 0.5–20 μmol/L and LOD of 58 nmol/L (21.37 ng/mL) [123]. In another study, Han et al. fabricated excitation-independent blue emission N and S co-doped CQDs with QY of 26.9% by using hydrothermal treatment (4 h at 180 °C) with precursors such as sodium citrate and thiourea [180]. Herein, the fluorescence of the CQDs was effectively quenched when curcumin is introduced into the solution (based on IFE), and hence, these CQDs can be used as switch "Off" fluorescent probe for curcumin detection in the range of 0.15–18.0 μmol/L with LOD of 0.04μmol/L. Furthermore, curcumin was efficiently detected in urine samples via N and S co-doped CQDs. In another investigation, Wu et al. prepared B, N, and P co-doped CQDs with QY of 21.95% (via hydrothermal reaction (10 h at 180 °C)of ethylenediamine, H_3PO_4 and 4-amino-phenylboronic acid), that have possessed remarkable selectivity and sensitivity towards curcumin with the linear range of 0–1.5 mmol/L and LOD of 68 nmol/L [181].

3.3.3. Detection of Pesticides and Fungicides

Pesticides and fungicides might be present at low levels in the food and environment, which could be highly dangerous for humans, and it is needed to detect them effectively. Recently, Li et al. developed N and S co-doped CQDs via pyrolysis (1 h at 450 °C) of an ionic liquid N-methylethanolammoniumthioglycolate, and used them efficiently as a sensor to detect residues of a pesticide—carbaryl [182]. Herein, carbaryl is detected sensitively (under the presence of acetylcholinesterase (AChE) and choline oxidase (ChOx)) in the concentration range of 6.3×10^{-9} g/L to 6.3×10^{-4} g/L with LOD of 5.4×10^{-9} g/L. Similarly in another study, Li et al. have employed N

and P co-doped CQDs as a fluorescent platform for the detection of carbendazim (a fungicide), which resulted in a good linear detection range from 0.005–0.16 µM with LOD of 0.002 µM [126].

3.4. Gene Delivery

It is highly necessary to deliver nucleic acids for therapeutic purposes. Recently, Zuo et al. prepared F-doped cationic CQDs (without/with branched PEI (b-PEI) of 1.8 K or 25 K) that achieved dramatic plasmid enhanced green fluorescent protein (pEGFP DNA) and luciferase gene transfection efficiency [66]. Herein, based on agarose gel electrophoresis retardation assay, it has been noted that the binding ratio of 1.8k b-PEI based F-doped CQDs to DNA is higher than that of only F-doped CQDs to EGFP plasmid DNA, which could be ascribed to the increased positive charge/molecular weight ratio of b-PEI based F-doped CQDs. In addition, the weight ratio of 25kb-PEI based F-doped CQDs to DNA is nearly equal to 0.5, indicating an equivalent binding capacity to that of only F-doped CQDs. Similarly, the results from the investigation by Luo et al. have revealed that the F-doped CQDs have possessed much higher transfection efficiency of pEGFP-N1 than PEI 600 contrasts in different cell lines including A549 cells, HepG2 cells, 7702 cells, and HeLa cells [67]. Moreover, as compared to non-fluorinated counterparts, the fluorinated CQDs have exhibited distinctly higher transfection efficiency, and up to 30 and 260 times higher efficiency than PEI 25 kDa is achieved in the absence and presence of serum, respectively, indicating the advantage of F-doping. Analogously, Chandra et al. made S-doped CQDs modified to possess 25 k b-PEI and PUC 19 (a DNA) on their surface to create DNA–PEI–CQDs complex based on positive and negative charge based electrostatic interactions [99]. Herein, the complex has emitted bright blue fluorescence at an excitation wavelength of 405 nm.

3.5. Temperature Probe

Han et al. utilized hydrothermal treatment (4 h at 180 °C) of the precursors such as sodium citrate and thiourea to produce N and S co-doped CQDs (with blue emission and QY of 26.9%) that showed a distinct temperature-sensitive phenomenon [180]. Moreover, these co-doped CQDs are used to fabricate a temperature sensor whose fluorescence has gradually quenched/decremented with the increase in temperature over a wide range from 5–70 °C. The authors have proposed two possible quenching mechanisms: (i) the synergistic effect of hydrogen bonds and abundant functional groups on the surface of N and S co-doped CQDs, which have made it possible to portray quick and sensitive response to the change in temperature, and (ii) the aggregation of these CQDs with the increment in temperature. Analogously in a recent study, Zuo et al. stated that owing to the pronounced temperature dependence of the fluorescence emission spectra, the resultant N and S co-doped CQDs can work as versatile nanothermometry devices by taking advantage of the temperature (5 to 80 °C) sensitivity of their emission intensity (F/F_0)—as shown in Figure 20 [183]. In another investigation, Shi et al. used the N and S co-doped CQDs as an effective temperature indicator that has exhibited good temperature-dependent fluorescence with a sensational linear response from 20 to 80 °C [184].
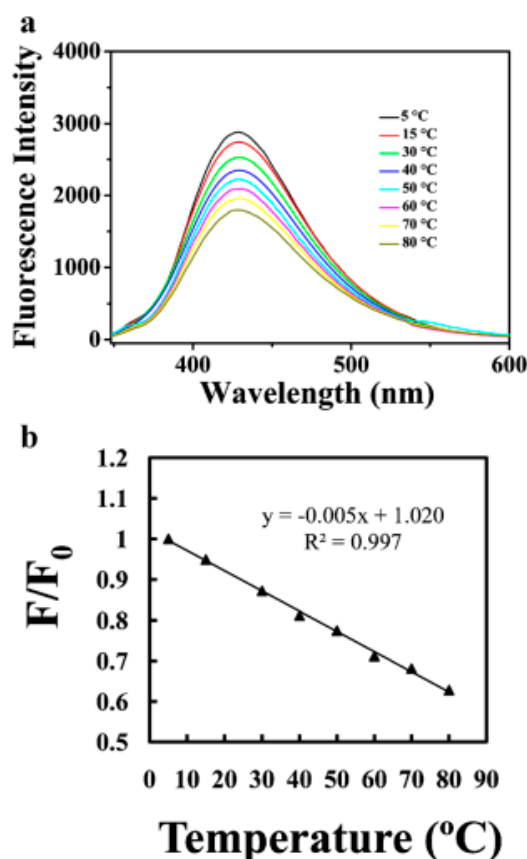
Figure 20. Fluorescence of the N and S co-doped CQDs against different temperatures excited at 340 nm (**a**) and normalized fluorescence intensities (F/F0)versus temperature (from 5–80 °C) (**b**). Reproduced with permission from Zuo et al. [183] Copyright Springer-Verlag GmbH Germany, part of Springer Nature, 2019.

4. Conclusions and Future Perspectives

To summarize, it can be noted that there are large number of investigations that involve in the effective preparation and optimization of doped and co-doped CQDs. The hydrothermal method is highly utilized in the synthesis of these doped and co-doped CQDs in comparison to other synthesis methods. Nevertheless, there are more avenues to explore in the preparation and optimization of these doped and co-doped CQDs via different synthesis protocols in near future, when comparing with the preparation methods of normal CQDs (without doping).

Moreover, based on the above discussed research-investigations, a lucid observation is that (i) the precursors along with the type of synthesis method (including the reaction conditions such as reaction time and/or temperature) and (ii) the type of doping have a great impact on the resultant quantum yield (QY) of the as-synthesized doped and co-doped CQDs. However, in many research studies, the reasons behind the enhancements in the QY in the doped and co-doped CQDs as compared to the normal CQDs are not completely evaluated. Thus, in near-future, it should be possible to clearly understand the inherent photoluminescence phenomenon in the doped and co-doped CQDs.

Furthermore, above 85% of the as-synthesized doped and co-doped CQDs has emitted blue fluorescence. Hence, the doped and co-doped CQDs with multi-color emissive properties can be explored and consequently utilized in different applications in future.

Besides the above, it has been confirmed that the doped and co-doped CQDs can be effectively utilized in different applications including electrical/electronics (such as LED and solar cells), fluorescent ink for anti-counterfeiting, optical sensors (for detection of metal ions, drugs, and pesticides/fungicides) including molecular logic gates, gene delivery, and temperature probing. However, the extent of

exploitation of these doped and co-doped CQDs in a wide variety of applications (including the biological applications) is less in comparison to the normal CQDs and to the other nanoparticles (e.g., superparamagnetic iron oxide nanoparticles (SPIONs)). Based on the above-given research studies, it can be concluded that the doped and co-doped CQDs are potential candidates for emerging applications.

Conflicts of Interest: The authors declare no conflict of interest.

References

1. Xu, X.; Ray, R.; Gu, Y.; Ploehn, H.J.; Gearheart, L.; Raker, K.; Scrivens, W.A. Electrophoretic Analysis and Purification of Fluorescent Single-Walled Carbon Nanotube Fragments. *J. Am. Chem. Soc.* **2004**, *126*, 12736–12737. [CrossRef]

2. Sun, Y.P.; Zhou, B.; Lin, Y.; Wang, W.; Fernando, K.A.S.; Pathak, P.; Meziani, M.J.; Harruff, B.A.; Wang, X.; Wang, H.; et al. Quantum-sized carbon dots for bright and colorful photoluminescence. *J. Am. Chem. Soc.* **2006**, *128*, 7756–7757. [CrossRef]

3. Cao, L.; Wang, X.; Meziani, M.J.; Lu, F.; Wang, H.; Luo, P.G.; Lin, Y.; Harruff, B.A.; Veca, L.M.; Murray, D.; et al. Carbon Dots for Multiphoton Bioimaging. *J. Am. Chem. Soc.* **2007**, *129*, 11318–11319. [CrossRef]

4. Yang, S.-T.; Cao, L.; Luo, P.G.; Lu, F.; Wang, X.; Wang, H.; Meziani, M.J.; Liu, Y.; Qi, G.; Sun, Y.-P. Carbon dots for optical imaging in vivo. *J. Am. Chem. Soc.* **2009**, *131*, 11308–11309. [CrossRef]

5. Liu, H.; Ye, T.; Mao, C. Fluorescent carbon nanoparticles derived from candle soot. *Angew. Chem. Int. Ed.* **2007**, *46*, 6473–6475. [CrossRef]

6. Bourlinos, A.B.; Stassinopoulos, A.; Anglos, D.; Zboril, R.; Karakassides, M.; Giannelis, E.P. Surface functionalized carbogenic quantum dots. *Small* **2008**, *4*, 455–458. [CrossRef]

7. Bourlinos, A.B.; Stassinopoulos, A.; Anglos, D.; Zboril, R.; Georgakilas, V.; Giannelis, E.P. Photoluminescent carbogenic dots. *Chem. Mater.* **2008**, *20*, 4539–4541. [CrossRef]

8. Liu, R.; Wu, D.; Liu, S.; Koynov, K.; Knoll, W.; Li, Q. An Aqueous Route to Multicolor Photoluminescent Carbon Dots Using Silica Spheres as Carriers. *Angew. Chem. Int. Ed.* **2009**, *48*, 4598–4601. [CrossRef]

9. Ray, S.C.; Saha, A.; Jana, N.R.; Sarkar, R. Fluorescent Carbon Nanoparticles: Synthesis, Characterization, and Bioimaging Application. *J. Phys. Chem. C* **2009**, *113*, 18546–18551. [CrossRef]

10. Tian, L.; Ghosh, D.; Chen, W.; Pradhan, S.; Chang, X.; Chen, S. Nanosized Carbon Particles From Natural Gas Soot. *Chem. Mater.* **2009**, *21*, 2803–2809. [CrossRef]

11. Zhu, H.; Wang, X.; Li, Y.; Wang, Z.; Yang, F.; Yang, X. Microwave synthesis of fluorescent carbon nanoparticles with electrochemiluminescence properties. *Chem. Commun.* **2009**, 5118–5120. [CrossRef]

12. Pan, D.; Zhang, J.; Li, Z.; Wu, C.; Yan, X.; Wu, M. Observation of pH-, solvent-, spin-, and excitation-dependent blue photoluminescence from carbon nanoparticles. *Chem. Commun.* **2010**, *46*, 3681–3683. [CrossRef]

13. Wang, F.; Pang, S.; Wang, L.; Li, Q.; Kreiter, M.; Liu, C.Y. One-step synthesis of highly luminescent carbon dots in noncoordinating solvents. *Chem. Mater.* **2010**, *22*, 4528–4530. [CrossRef]

14. Zhang, B.; Liu, C.; Liu, Y. A Novel One-Step Approach to Synthesize Fluorescent Carbon Nanoparticles. *Eur. J. Inorg. Chem.* **2010**, *2010*, 4411–4414. [CrossRef]

15. Yang, Z.-C.; Wang, M.; Yong, A.M.; Wong, S.Y.; Zhang, X.-H.; Tan, H.; Chang, A.Y.; Li, X.; Wang, J. Intrinsically fluorescent carbon dots with tunable emission derived from hydrothermal treatment of glucose in the presence of monopotassium phosphate. *Chem. Commun.* **2011**, *47*, 11615–11617. [CrossRef]

16. Li, H.; He, X.; Kang, Z.; Huang, H.; Liu, Y.; Liu, J.; Lian, S.; Tsang, C.H.A.; Yang, X.; Lee, S.T. Water-soluble fluorescent carbon quantum dots and photocatalyst design. *Angew. Chem. Int. Ed.* **2010**, *49*, 4430–4434. [CrossRef]

17. Li, H.; He, X.; Liu, Y.; Huang, H.; Lian, S.; Lee, S.T.; Kang, Z. One-step ultrasonic synthesis of water-soluble carbon nanoparticles with excellent photoluminescent properties. *Carbon* **2011**, *49*, 605–609. [CrossRef]

18. Lu, A.H.; Hao, G.P.; Sun, Q. Can carbon spheres be created through the stöber method? *Angew. Chem. Int. Ed.* **2011**, *50*, 9023–9025. [CrossRef]

19. Sahu, S.; Behera, B.; Maiti, T.K.; Mohapatra, S. Simple one-step synthesis of highly luminescent carbon dots from orange juice: Application as excellent bio-imaging agents. *Chem. Commun.* **2012**, *48*, 8835. [CrossRef]

20. Wang, F.; Xie, Z.; Zhang, B.; Liu, Y.; Yang, W.; Liu, C. Down- and up-conversion luminescent carbon dot fluid: Inkjet printing and gel glass fabrication. *Nanoscale* **2014**, *6*, 3818–3823. [CrossRef]

21. Liu, Y.; Xiao, N.; Gong, N.; Wang, H.; Shi, X.; Gu, W.; Ye, L. One-step microwave-assisted polyol synthesis of green luminescent carbon dots as optical nanoprobes. *Carbon* **2014**, *68*, 258–264. [CrossRef]

22. Baker, S.N.; Baker, G.A. Luminescent carbon nanodots: Emergent nanolights. *Angew. Chem. Int. Ed.* **2010**, *49*, 6726–6744. [CrossRef]

23. Esteves da Silva, J.C.G.; Gonçalves, H.M.R. Analytical and bioanalytical applications of carbon dots. *TrAC Trends Anal. Chem.* **2011**, *30*, 1327–1336. [CrossRef]

24. Dimos, K. Carbon Quantum Dots: Surface Passivation and Functionalization. *Curr. Org. Chem.* **2016**, *20*, 682–695. [CrossRef]

25. Park, Y.; Yoo, J.; Lim, B.; Kwon, W.; Rhee, S.-W. Improving Functionality of Carbon Nanodots: Doping and Surface Functionalization. *J. Mater. Chem. A* **2016**, *4*, 11582–11603. [CrossRef]

26. Das, A.; Snee, P.T. Synthetic Developments of Nontoxic Quantum Dots. *ChemPhysChem* **2016**, *17*, 598–617. [CrossRef]

27. Wang, F.; Chen, Y.; Liu, C.; Ma, D. White light-emitting devices based on carbon dots' electroluminescence. *Chem. Commun.* **2011**, *47*, 3502. [CrossRef]

28. Li, H.; Kang, Z.; Liu, Y.; Lee, S.-T. Carbon nanodots: Synthesis, properties and applications. *J. Mater. Chem.* **2012**, *22*, 24230. [CrossRef]

29. Gao, X.; Du, C.; Zhuang, Z.; Chen, W. Carbon quantum dot-based nanoprobes for metal ion detection. *J. Mater. Chem. C* **2016**, *4*, 6927–6945. [CrossRef]

30. Grumezescu, A.M. *Nanobiomaterials in Medical Imaging: Applications of Nanobiomaterials*; Elsevier: Amsterdam, The Netherlands, 2016; ISBN 9780323417365.

31. Guo, Y.; Zhang, L.; Zhang, S.; Yang, Y.; Chen, X.; Zhang, M. Fluorescent carbon nanoparticles for the fluorescent detection of metal ions. *Biosens. Bioelectron.* **2015**, *63*, 61–71. [CrossRef]

32. Roy, P.; Chen, P.C.; Periasamy, A.P.; Chen, Y.N.; Chang, H.T. Photoluminescent carbon nanodots: Synthesis, physicochemical properties and analytical applications. *Mater. Today* **2015**, *18*, 447–458. [CrossRef]

33. Miao, P.; Han, K.; Tang, Y.; Wang, B.; Lin, T.; Cheng, W. Recent advances in carbon nanodots: Synthesis, properties and biomedical applications. *Nanoscale* **2015**, *7*, 1586–1595. [CrossRef]

34. Yang, Z.; Li, Z.; Xu, M.; Xu, M.; Ma, Y.; Zhang, J.; Su, Y.; Su, Y.; Gao, F.; Wei, H.; et al. Controllable Synthesis of Fluorescent Carbon Dots and Their Detection Application as Nanoprobes. *Nano-Micro Lett.* **2013**, *5*, 247–259. [CrossRef]

35. Zhang, J.; Yu, S.-H. Carbon dots: Large-scale synthesis, sensing and bioimaging. *Mater. Today* **2015**, *19*, 382–393. [CrossRef]

36. Ding, C.; Zhu, A.; Tian, Y. Functional surface engineering of C-dots for fluorescent biosensing and in vivo bioimaging. *Acc. Chem. Res.* **2014**, *47*, 20–30. [CrossRef]

37. Xu, Y.; Liu, J.; Gao, C.; Wang, E. Applications of carbon quantum dots in electrochemiluminescence: A mini review. *Electrochem. Commun.* **2014**, *48*, 151–154. [CrossRef]

38. Yuan, L.; Dai, J.; Fan, X.; Song, T.; Tao, Y.T.; Wang, K.; Xu, Z.; Zhang, J.; Bai, X.; Lu, P.; et al. Self-cleaning flexible infrared nanosensor based on carbon nanoparticles. *ACS Nano* **2011**, *5*, 4007–4013. [CrossRef]

39. Zhu, L.; Yin, Y.; Wang, C.-F.; Chen, S. Plant leaf-derived fluorescent carbon dots for sensing, patterning and coding. *J. Mater. Chem. C* **2013**, *1*, 4925–4932. [CrossRef]

40. Jiang, Y.; Wei, G.; Zhang, W.; Wang, Z.; Cheng, Y.; Dai, Z. Solid phase reaction method for preparation of carbon dots and multi-purpose applications. *Sens. Actuators B Chem.* **2016**, *234*, 15–20. [CrossRef]

41. Zhang, J.; Cheng, F.; Li, J.; Zhu, J.-J.; Lu, Y. Fluorescent nanoprobes for sensing and imaging of metal ions: Recent advances and future perspectives. *Nano Today* **2016**, *11*, 309–329. [CrossRef]

42. Du, Y.; Guo, S. Chemically doped fluorescent carbon and graphene quantum dots for bioimaging, sensor, catalytic and photoelectronic applications. *Nanoscale* **2016**, *8*, 2532–2543. [CrossRef]

43. Li, X.; Rui, M.; Song, J.; Shen, Z.; Zeng, H. Carbon and Graphene Quantum Dots for Optoelectronic and Energy Devices: A Review. *Adv. Funct. Mater.* **2015**, *25*, 4929–4947. [CrossRef]

44. Zuo, J.; Jiang, T.; Zhao, X.; Xiong, X.; Xiao, S.; Zhu, Z. Preparation and Application of Fluorescent Carbon Dots. *J. Nanomater.* **2015**, *2015*, 1–13. [CrossRef]

45. Wang, Q.; Huang, X.; Long, Y.; Wang, X.; Zhang, H.; Zhu, R.; Liang, L.; Teng, P.; Zheng, H. Hollow luminescent carbon dots for drug delivery. *Carbon* **2013**, *59*, 192–199. [CrossRef]

46. Zhao, A.; Chen, Z.; Zhao, C.; Gao, N.; Ren, J.; Qu, X. Recent advances in bioapplications of C-dots. *Carbon* **2015**, *85*, 309–327. [CrossRef]

47. Hong, G.; Diao, S.; Antaris, A.L.; Dai, H. Carbon Nanomaterials for Biological Imaging and Nanomedicinal Therapy. *Chem. Rev.* **2015**, *115*, 10816–10906. [CrossRef]

48. Lim, S.Y.; Shen, W.; Gao, Z. Carbon quantum dots and their applications. *Chem. Soc. Rev.* **2014**, *44*, 362–381. [CrossRef]

49. Das, R.; Bandyopadhyay, R.; Pramanik, P. Carbon quantum dots from natural resource: A review. *Mater. Today Chem.* **2018**, *8*, 96–109. [CrossRef]

50. Hola, K.; Zhang, Y.; Wang, Y.; Giannelis, E.P.; Zboril, R.; Rogach, A.L. Carbon dots—Emerging light emitters for bioimaging, cancer therapy and optoelectronics. *Nano Today* **2014**, *9*, 590–603. [CrossRef]

51. De, B.; Karak, N. A green and facile approach for the synthesis of water soluble fluorescent carbon dots from banana juice. *RSC Adv.* **2013**, *3*, 8286. [CrossRef]

52. Hu, X.; Cheng, L.; Wang, N.; Sun, L.; Wang, W.; Liu, W. Surface passivated carbon nanodots prepared by microwave assisted pyrolysis: Effect of carboxyl group in precursors on fluorescence properties. *RSC Adv.* **2014**, *4*, 18818. [CrossRef]

53. Li, J.; Zhu, J.-J. Quantum dots for fluorescent biosensing and bio-imaging applications. *Analyst* **2013**, *138*, 2506. [CrossRef] [PubMed]

54. Gnaneshwar, P.V.; Sabarikirishwaran, P. Structural and morphological study of carbon nanoparticles synthesized using oxidation, thermal decomposition and solvo chemical methods. *Int. J. ChemTech Res.* **2015**, *7*, 1465–1473.

55. Li, F.; Yang, D.; Xu, H. Non-Metal-Heteroatom-Doped Carbon Dots: Synthesis and Properties. *Chem. A Eur. J.* **2019**, *25*, 1165–1176. [CrossRef] [PubMed]

56. Li, L.; Dong, T. Photoluminescence tuning in carbon dots: Surface passivation or/and functionalization, heteroatom doping. *J. Mater. Chem. C* **2018**, *6*, 7944–7970. [CrossRef]

57. Jana, J.; Pal, T. An account of doping in carbon dots for varied applications. *Nat. Resour. Eng.* **2018**, *2*, 5–12. [CrossRef]

58. Atabaev, T. Doped Carbon Dots for Sensing and Bioimaging Applications: A Minireview. *Nanomaterials* **2018**, *8*, 342. [CrossRef]

59. Wolfbeis, O.S. An overview of nanoparticles commonly used in fluorescent bioimaging. *Chem. Soc. Rev. Chem. Soc Rev* **2015**, *44*, 4743–4768. [CrossRef]

60. Lin, L.; Luo, Y.; Tsai, P.; Wang, J.; Chen, X. Metal ions doped carbon quantum dots: Synthesis, physicochemical properties, and their applications. *TrAC Trends Anal. Chem.* **2018**, *103*, 87–101. [CrossRef]

61. Shan, X.; Chai, L.; Ma, J.; Qian, Z.; Chen, J.; Feng, H. B-doped carbon quantum dots as a sensitive fluorescence probe for hydrogen peroxide and glucose detection. *Analyst* **2014**, *139*, 2322–2325. [CrossRef]

62. Bourlinos, A.B.; Trivizas, G.; Karakassides, M.A.; Baikousi, M.; Kouloumpis, A.; Gournis, D.; Bakandritsos, A.; Hola, K.; Kozak, O.; Zboril, R.; et al. Green and simple route toward boron doped carbon dots with significantly enhanced non-linear optical properties. *Carbon* **2015**, *83*, 173–179. [CrossRef]

63. Jana, J.; Ganguly, M.; Chandrakumar, K.R.S.; Rao, G.M.; Pal, T. Boron precursor-dependent evolution of differently emitting carbon dots. *Langmuir* **2017**, *33*, 573–584. [CrossRef] [PubMed]

64. Jia, Y.; Hu, Y.; Li, Y.; Zeng, Q.; Jiang, X.; Cheng, Z. Boron doped carbon dots as a multifunctional fluorescent probe for sorbate and vitamin B12. *Microchim. Acta* **2019**, *186*, 4–13. [CrossRef] [PubMed]

65. Zuo, G.; Xie, A.; Li, J.; Su, T.; Pan, X.; Dong, W. Large Emission Red-Shift of Carbon Dots by Fluorine Doping and Their Applications for Red Cell Imaging and Sensitive Intracellular Ag+ Detection. *J. Phys. Chem. C* **2017**, *121*, 26558–26565. [CrossRef]

66. Zuo, G.; Xie, A.; Pan, X.; Su, T.; Li, J.; Dong, W. Fluorine-Doped Cationic Carbon Dots for Efficient Gene Delivery. *ACS Appl. Nano Mater.* **2018**, *1*, 2376–2385. [CrossRef]

67. Luo, T.Y.; He, X.; Zhang, J.; Chen, P.; Liu, Y.H.; Wang, H.J.; Yu, X.Q. Photoluminescent F-doped carbon dots prepared by ring-opening reaction for gene delivery and cell imaging. *RSC Adv.* **2018**, *8*, 6053–6062. [CrossRef]

68. Liu, S.; Tian, J.; Wang, L.; Zhang, Y.; Qin, X.; Luo, Y.; Asiri, A.M.; Al-Youbi, A.O.; Sun, X. Hydrothermal Treatment of Grass: A Low-Cost, Green Route to Nitrogen-Doped, Carbon-Rich, Photoluminescent Polymer Nanodots as an Effective Fluorescent Sensing Platform for Label-Free Detection of Cu(II) Ions. *Adv. Mater.* **2012**, *24*, 2037–2041. [CrossRef]

69. Dey, S.; Chithaiah, P.; Belawadi, S.; Biswas, K.; Rao, C.N.R. New methods of synthesis and varied properties of carbon quantum dots with high nitrogen content. *J. Mater. Res.* **2014**, *29*, 383–391. [CrossRef]

70. Wang, L.; Yin, Y.; Jain, A.; Susan Zhou, H. Aqueous phase synthesis of highly luminescent, nitrogen-doped carbon dots and their application as bioimaging agents. *Langmuir* **2014**, *30*, 14270–14275. [CrossRef]

71. Niu, J.; Gao, H. Synthesis and drug detection performance of nitrogen-doped carbon dots. *J. Lumin.* **2014**, *149*, 159–162. [CrossRef]

72. Qian, Z.; Ma, J.; Shan, X.; Feng, H.; Shao, L.; Chen, J. Highly luminescent N-doped carbon quantum dots as an effective multifunctional fluorescence sensing platform. *Chem. A Eur. J.* **2014**, *20*, 2254–2263. [CrossRef] [PubMed]

73. Zhang, H.; Li, Y.; Liu, X.; Liu, P.; Wang, Y.; An, T.; Yang, H.; Jing, D.; Zhao, H. Determination of Iodide via Direct Fluorescence Quenching at Nitrogen-Doped Carbon Quantum Dot Fluorophores. *Environ. Sci. Technol. Lett.* **2013**, *1*, 87–91. [CrossRef]

74. Campos, B.B.; Abellán, C.; Zougagh, M.; Jimenez-Jimenez, J.; Rodríguez-Castellón, E.; Esteves da Silva, J.C.G.; Ríos, A.; Algarra, M. Fluorescent chemosensor for pyridine based on N-doped carbon dots. *J. Colloid Interface Sci.* **2015**, *458*, 209–216. [CrossRef] [PubMed]

75. Lv, P.; Yao, Y.; Zhou, H.; Zhang, J.; Pang, Z.; Ao, K.; Cai, Y.; Wei, Q. Synthesis of novel nitrogen-doped carbon dots for highly selective detection of iron ion. *Nanotechnology* **2017**, *28*, 165502. [CrossRef] [PubMed]

76. Wu, F.; Su, H.; Wang, K.; Wong, W.-K.; Zhu, X. Facile synthesis of N-rich carbon quantum dots from porphyrins as efficient probes for bioimaging and biosensing in living cells. *Int. J. Nanomed.* **2017**, *12*, 7375–7391. [CrossRef] [PubMed]

77. Hu, R.; Li, L.; Jin, W.J. Controlling speciation of nitrogen in nitrogen-doped carbon dots by ferric ion catalysis for enhancing fluorescence. *Carbon* **2017**, *111*, 133–141. [CrossRef]

78. Ding, H.; Zhang, P.; Wang, T.Y.; Kong, J.L.; Xiong, H.M. Nitrogen-doped carbon dots derived from polyvinyl pyrrolidone and their multicolor cell imaging. *Nanotechnology* **2014**, *25*, 205604. [CrossRef]

79. Wang, H.; Gao, P.; Wang, Y.; Guo, J.; Zhang, K.-Q.; Du, D.; Dai, X.; Zou, G. Fluorescently tuned nitrogen-doped carbon dots from carbon source with different content of carboxyl groups. *APL Mater.* **2015**, *3*, 086102. [CrossRef]

80. Jiang, K.; Sun, S.; Zhang, L.; Wang, Y.; Cai, C.; Lin, H. Bright-Yellow-Emissive N-Doped Carbon Dots: Preparation, Cellular Imaging, and Bifunctional Sensing. *ACS Appl. Mater. Interfaces* **2015**, *7*, 23231–23238. [CrossRef]

81. Ji, H.; Zhou, F.; Gu, J.; Shu, C.; Xi, K.; Jia, X. Nitrogen-doped carbon dots as a new substrate for sensitive glucose determination. *Sensors* **2016**, *16*, 1–10. [CrossRef]

82. Li, M.; Huang, J.; Fan, H.; Ding, H.; Huang, K.; Huang, L.; Xu, L.; Xia, J.; Li, S. Eosinophilic nitrogen-doped carbon dots derived from tribute chrysanthemum for label-free detection of Fe^{3+} ions and hydrazine. *J. Taiwan Inst. Chem. Eng.* **2017**, *78*, 247–253.

83. Jiang, X.; Qin, D.; Mo, G.; Feng, J.; Yu, C.; Mo, W.; Deng, B. Ginkgo leaf-based synthesis of nitrogen-doped carbon quantum dots for highly sensitive detection of salazosulfapyridine in mouse plasma. *J. Pharm. Biomed. Anal.* **2019**, *164*, 514–519. [CrossRef] [PubMed]

84. Wang, R.; Wang, X.; Sun, Y. One-step synthesis of self-doped carbon dots with highly photoluminescence as multifunctional biosensors for detection of iron ions and pH. *Sens. Actuators B Chem.* **2017**, *241*, 73–79. [CrossRef]

85. Wu, P.; Li, W.; Wu, Q.; Liu, Y.; Liu, S. Hydrothermal synthesis of nitrogen-doped carbon quantum dots from microcrystalline cellulose for the detection of Fe3+ ions in an acidic environment. *RSC Adv.* **2017**, *7*, 44144–44153. [CrossRef]

86. Hou, J.; Wang, W.; Zhou, T.; Wang, B.; Li, H.; Ding, L. Synthesis and formation mechanistic investigation of nitrogen-doped carbon dots with high quantum yield and yellowish-green fluorescence. *Nanoscale* **2016**, *8*, 11185–11193. [CrossRef] [PubMed]

87. Zhu, S.; Meng, Q.; Wang, L.; Zhang, J.; Song, Y.; Jin, H.; Zhang, K.; Sun, H.; Wang, H.; Yang, B. Highly photoluminescent carbon dots for multicolor patterning, sensors, and bioimaging. *Angew. Chem. Int. Ed.* **2013**, *52*, 3953–3957. [CrossRef] [PubMed]

88. Tang, Y.; Rao, L.; Li, Z.; Lu, H.; Yan, C.; Yu, S.; Ding, X.; Yu, B. Rapid synthesis of highly photoluminescent nitrogen-doped carbon quantum dots via a microreactor with foamy copper for the detection of Hg2+ ions. *Sens. Actuators B Chem.* **2018**, *258*, 637–647. [CrossRef]

89. Zheng, M.; Xie, Z.; Qu, D.; Li, D.; Du, P.; Jing, X.; Sun, Z. On-off-on fluorescent carbon dot nanosensor for recognition of chromium(VI) and ascorbic acid based on the inner filter effect. *ACS Appl. Mater. Interfaces* **2013**, *5*, 13242–13247. [CrossRef] [PubMed]

90. Meiling, T.T.; Schürmann, R.; Vogel, S.; Ebel, K.; Nicolas, C.; Milosavljević, A.R.; Bald, I. Photophysics and Chemistry of Nitrogen-Doped Carbon Nanodots with High Photoluminescence Quantum Yield. *J. Phys. Chem. C* **2018**, *122*, 10217–10230. [CrossRef]

91. Zhou, J.; Shan, X.; Ma, J.; Gu, Y.; Qian, Z.; Chen, J.; Feng, H. Facile synthesis of P-doped carbon quantum dots with highly efficient photoluminescence. *RSC Adv.* **2014**, *4*, 5465–5468. [CrossRef]

92. Shi, D.; Yan, F.; Zheng, T.; Wang, Y.; Zhou, X.; Chen, L. P-doped carbon dots act as a nanosensor for trace 2,4,6-trinitrophenol detection and a fluorescent reagent for biological imaging. *RSC Adv.* **2015**, *5*, 98492–98499. [CrossRef]

93. Sarkar, S.; Das, K.; Ghosh, M.; Das, P.K. Amino acid functionalized blue and phosphorous-doped green fluorescent carbon dots as bioimaging probe. *RSC Adv.* **2015**, *5*, 65913–65921. [CrossRef]

94. Li, Y.; Lin, H.; Luo, C.; Wang, Y.; Jiang, C.; Qi, R.; Huang, R.; Travas-sejdic, J.; Peng, H. Aggregation induced red shift emission of phosphorus doped carbon dots. *RSC Adv.* **2017**, *7*, 32225–32228. [CrossRef]

95. Chen, Z.; Wang, S.; Yang, X. Phosphorus-doped carbon dots for sensing both Au (III) and L-methionine. *J. Photochem. Photobiol. A Chem.* **2018**, *365*, 178–184. [CrossRef]

96. Yang, F.; He, X.; Wang, C.; Cao, Y.; Li, Y.; Yan, L.; Liu, M.; Lv, M.; Yang, Y.; Zhao, X.; et al. *Controllable and Eco-Friendly Synthesis of P-Riched Carbon Quantum Dots and Its Application for Copper (II) Ion Sensing*; Elsevier B.V.: Amsterdam, The Netherlands, 2018; Volume 448, ISBN 8601089739.

97. Wang, W.; Li, Y.; Cheng, L.; Cao, Z.; Liu, W. Water-soluble and phosphorus-containing carbon dots with strong green fluorescence for cell labeling. *J. Mater. Chem. B* **2014**, *2*, 46–48. [CrossRef]

98. Omer, K.M.; Hassan, A.Q. Chelation-enhanced fluorescence of phosphorus doped carbon nanodots for multi-ion detection. *Microchim. Acta* **2017**, *184*, 2063–2071. [CrossRef]

99. Chandra, S.; Patra, P.; Pathan, S.H.; Roy, S.; Mitra, S.; Layek, A.; Bhar, R.; Pramanik, P.; Goswami, A. Luminescent S-doped carbon dots: An emergent architecture for multimodal applications. *J. Mater. Chem. B* **2013**, *1*, 2375–2382. [CrossRef]

100. Hu, Y.; Yang, J.; Tian, J.; Jia, L.; Yu, J.S. Waste frying oil as a precursor for one-step synthesis of sulfur-doped carbon dots with pH-sensitive photoluminescence. *Carbon* **2014**, *77*, 775–782. [CrossRef]

101. Xu, Q.; Pu, P.; Zhao, J.; Dong, C.; Gao, C.; Chen, Y.; Chen, J.; Liu, Y.; Zhou, H. Preparation of highly photoluminescent sulfur-doped carbon dots for Fe(III) detection. *J. Mater. Chem. A* **2015**, *3*, 542–546. [CrossRef]

102. Dany Rahmayanti, H.; Sulhadi; Aji, M.P. Synthesis of Sulfur-Doped Carbon Dots by Simple Heating Method. *Adv. Mater. Res.* **2015**, *1123*, 233–236. [CrossRef]

103. Yang, H.; Li, F.; Zou, C.; Huang, Q.; Chen, D. Sulfur-doped carbon quantum dots and derived 3D carbon nanoflowers are effective visible to near infrared fluorescent probes for hydrogen peroxide. *Microchim. Acta* **2017**, *184*, 2055–2062. [CrossRef]

104. Travlou, N.A.; Secor, J.; Bandosz, T.J. Highly luminescent S-doped carbon dots for the selective detection of ammonia. *Carbon* **2017**, *114*, 544–556. [CrossRef]

105. Loukanov, A.; Mladenova, P.; Udono, H.; Miskolczy, Z.; Angelov, A.; Biczók, L.; Nakabayashi, S. Sulfur doped fluorescent carbon dots as nanosensors for rapid and sensitive monitoring of calcium in hard water. *J. Chem. Technol. Metall.* **2018**, *53*, 473–479.

106. Pawar, S.P.; Anbhule, P.V.; Naik, V.M.; Kolekar, G.B.; Gunjal, D.B.; Gore, A.H.; Mahanwar, S.T. Quick and low cost synthesis of sulphur doped carbon dots by simple acidic carbonization of sucrose for the detection of Fe3+ ions in highly acidic environment. *Diam. Relat. Mater.* **2018**, *88*, 262–268.

107. Wu, F.; Yang, M.; Zhang, H.; Zhu, S.; Zhu, X.; Wang, K. Facile synthesis of sulfur-doped carbon quantum dots from vitamin B1 for highly selective detection of Fe^{3+} ion. *Opt. Mater.* **2018**, *77*, 258–263. [CrossRef]

108. Liu, J.; Li, J.; Xu, L.; Qiao, Y.; Chen, J. Facile Synthesis of N, B-Doped Carbon Dots and Their Application for Multisensor and Cellular Imaging. *Ind. Eng. Chem. Res.* **2017**, *56*, 3905–3912. [CrossRef]

109. Ye, Q.; Yan, F.; Shi, D.; Zheng, T.; Wang, Y.; Zhou, X.; Chen, L. N, B-doped carbon dots as a sensitive fluorescence probe for Hg^{2+} ions and 2,4,6-trinitrophenol detection for bioimaging. *J. Photochem. Photobiol. B Biol.* **2016**, *162*, 1–13. [CrossRef]

110. Guo, Y.; Chen, Y.; Cao, F.; Wang, L.; Wang, Z.; Leng, Y. Hydrothermal synthesis of nitrogen and boron doped carbon quantum dots with yellow-green emission for sensing Cr(VI), anti-counterfeiting and cell imaging. *RSC Adv.* **2017**, *7*, 48386–48393. [CrossRef]

111. Huang, S.; Yang, E.; Yao, J.; Liu, Y.; Xiao, Q. Carbon dots doped with nitrogen and boron as ultrasensitive fluorescent probes for determination of α-glucosidase activity and its inhibitors in water samples and living cells. *Microchim. Acta* **2018**, *185*, 3–11. [CrossRef] [PubMed]

112. Li, N.B.; Liu, S.G.; Li, N.; Mo, S.; Xiao, N.; Ju, Y.J.; Luo, H.Q.; Ling, Y. Highly selective detection of p-nitrophenol using fluorescence assay based on boron, nitrogen co-doped carbon dots. *Talanta* **2018**, *184*, 184–192.

113. Xiao, N.; Liu, S.G.; Mo, S.; Yang, Y.Z.; Han, L.; Ju, Y.J.; Li, N.B.; Luo, H.Q. B,N-carbon dots-based ratiometric fluorescent and colorimetric dual-readout sensor for H_2O_2 and H_2O_2-involved metabolites detection using $ZnFe_2O_4$ magnetic microspheres as peroxidase mimics. *Sens. Actuators B Chem.* **2018**, *273*, 1735–1743. [CrossRef]

114. Tian, T.; He, Y.; Ge, Y.; Song, G. One-pot synthesis of boron and nitrogen co-doped carbon dots as the fluorescence probe for dopamine based on the redox reaction between Cr(VI) and dopamine. *Sens. Actuators B Chem.* **2017**, *240*, 1265–1271. [CrossRef]

115. Zhao, C.; Jiao, Y.; Zhang, L.; Yang, Y. One-step synthesis of S,B co-doped carbon dots and their application for selective and sensitive fluorescence detection of diethylstilbestrol. *New J. Chem.* **2018**, *42*, 2857–2864. [CrossRef]

116. Yang, W.; Zhang, H.; Lai, J.; Peng, X.; Hu, Y.; Gu, W.; Ye, L. Carbon dots with red-shifted photoluminescence by fluorine doping for optical bio-imaging. *Carbon* **2018**, *128*, 78–85. [CrossRef]

117. Omer, K.M.; Tofiq, D.I.; Ghafoor, D.D. Highly photoluminescent label free probe for Chromium (II) ions using carbon quantum dots co-doped with nitrogen and phosphorous. *J. Lumin.* **2019**, *206*, 540–546. [CrossRef]

118. Huang, S.; Yang, E.; Liu, Y.; Yao, J.; Su, W.; Xiao, Q. Low-temperature rapid synthesis of nitrogen and phosphorus dual-doped carbon dots for multicolor cellular imaging and hemoglobin probing in human blood. *Sens. Actuators B Chem.* **2018**, *265*, 326–334. [CrossRef]

119. Liao, S.; Zhu, F.; Zhao, X.; Yang, H.; Chen, X. A reusable P, N-doped carbon quantum dot fluorescent sensor for cobalt ion. *Sens. Actuators B Chem.* **2018**, *260*, 156–164. [CrossRef]

120. Li, H.; Shao, F.Q.; Zou, S.Y.; Yang, Q.J.; Huang, H.; Feng, J.J.; Wang, A.J. Microwave-assisted synthesis of N,P-doped carbon dots for fluorescent cell imaging. *Microchim. Acta* **2016**, *183*, 821–826. [CrossRef]

121. Chandra, S.; Laha, D.; Pramanik, A.; Ray Chowdhuri, A.; Karmakar, P.; Sahu, S.K. Synthesis of highly fluorescent nitrogen and phosphorus doped carbon dots for the detection of Fe^{3+} ions in cancer cells. *Luminescence* **2016**, *31*, 81–87. [CrossRef]

122. Chandra, S.; Chowdhuri, A.R.; Laha, D.; Sahu, S.K. Fabrication of nitrogen- and phosphorous-doped carbon dots by the pyrolysis method for iodide and iron(III) sensing. *Luminescence* **2018**, *33*, 336–344. [CrossRef]

123. Liu, Y.; Gong, X.; Dong, W.; Zhou, R.; Shuang, S.; Dong, C. Nitrogen and phosphorus dual-doped carbon dots as a label-free sensor for Curcumin determination in real sample and cellular imaging. *Talanta* **2018**, *183*, 61–69. [CrossRef] [PubMed]

124. Omer, K.M.; Tofiq, D.I.; Hassan, A.Q. Solvothermal synthesis of phosphorus and nitrogen doped carbon quantum dots as a fluorescent probe for iron(III). *Microchim. Acta* **2018**, *185*, 4–11. [CrossRef] [PubMed]

125. Li, J.; Jiao, Y.; Feng, L.; Zhong, Y.; Zuo, G.; Xie, A.; Dong, W. Highly N,P-doped carbon dots: Rational design, photoluminescence and cellular imaging. *Microchim. Acta* **2017**, *184*, 2933–2940. [CrossRef]

126. Yang, Y.; Huo, D.; Wu, H.; Wang, X.; Yang, J.; Bian, M.; Ma, Y.; Hou, C. N, P-doped carbon quantum dots as a fluorescent sensing platform for carbendazim detection based on fluorescence resonance energy transfer. *Sens. Actuators B Chem.* **2018**, *274*, 296–303. [CrossRef]

127. Sun, X.; Brückner, C.; Lei, Y. One-pot and ultrafast synthesis of nitrogen and phosphorus co-doped carbon dots possessing bright dual wavelength fluorescence emission. *Nanoscale* **2015**, *7*, 17278–17282. [CrossRef] [PubMed]

128. Bao, R.; Chen, Z.; Zhao, Z.; Sun, X.; Zhang, J.; Hou, L.; Yuan, C. Green and Facile Synthesis of Nitrogen and Phosphorus Co-Doped Carbon Quantum Dots towards Fluorescent Ink and Sensing Applications. *Nanomaterials* **2018**, *8*, 386. [CrossRef] [PubMed]

129. Gong, Y.; Yu, B.; Yang, W.; Zhang, X. Phosphorus, and nitrogen co-doped carbon dots as a fluorescent probe for real-time measurement of reactive oxygen and nitrogen species inside macrophages. *Biosens. Bioelectron.* **2016**, *79*, 822–828. [CrossRef]

130. Shamsipur, M.; Molaei, K.; Molaabasi, F.; Hosseinkhani, S.; Alizadeh, N.; Alipour, M.; Moassess, S. One-step synthesis and characterization of highly luminescent nitrogen and phosphorus co-doped carbon dots and their application as highly selective and sensitive nanoprobes for low level detection of uranyl ion in hair and water samples and application. *Sens. Actuators B Chem.* **2018**, *257*, 772–782. [CrossRef]

131. Hu, Q.; Paau, M.C.; Zhang, Y.; Gong, X.; Zhang, L.; Lu, D.; Liu, Y.; Liu, Q.; Yao, J.; Choi, M.M.F. Green synthesis of fluorescent nitrogen/sulfur-doped carbon dots and investigation of their properties by HPLC coupled with mass spectrometry. *RSC Adv.* **2014**, *4*, 18065–18073. [CrossRef]

132. Akhgari, F.; Samadi, N.; Farhadi, K.; Akhgari, M. A green one-pot synthesis of nitrogen and sulfur co-doped carbon quantum dots for sensitive and selective detection of cephalexin. *Can. J. Chem.* **2017**, *95*, 641–648. [CrossRef]

133. Cheng, C.; Xing, M.; Wu, Q. A universal facile synthesis of nitrogen and sulfur co-doped carbon dots from cellulose-based biowaste for fluorescent detection of Fe3+ ions and intracellular bioimaging. *Mater. Sci. Eng. C* **2019**, *99*, 611–619. [CrossRef]

134. Simões, E.F.C.; Leitão, J.M.M.; Esteves da Silva, J.C.G. Sulfur and nitrogen co-doped carbon dots sensors for nitric oxide fluorescence quantification. *Anal. Chim. Acta* **2017**, *960*, 117–122. [CrossRef]

135. Wang, J.; Xiang, X.; Milcovich, G.; Chen, J.; Chen, C.; Feng, J.; Hudson, S.P.; Weng, X.; Ruan, Y. Nitrogen and sulfur co-doped carbon nanodots toward bovine hemoglobin: A fluorescence quenching mechanism investigation. *J. Mol. Recognit.* **2019**, *32*, 1–9. [CrossRef]

136. Chen, Y.; Wu, Y.; Weng, B.; Wang, B.; Li, C. Facile synthesis of nitrogen and sulfur co-doped carbon dots and application for Fe(III) ions detection and cell imaging. *Sens. Actuators B Chem.* **2016**, *223*, 689–696. [CrossRef]

137. Zhao, S.; Lan, M.; Zhu, X.; Xue, H.; Ng, T.W.; Meng, X.; Lee, C.S.; Wang, P.; Zhang, W. Green Synthesis of Bifunctional Fluorescent Carbon Dots from Garlic for Cellular Imaging and Free Radical Scavenging. *ACS Appl. Mater. Interfaces* **2015**, *7*, 17054–17060. [CrossRef]

138. Sun, C.; Zhang, Y.; Wang, P.; Yang, Y.; Wang, Y.; Xu, J.; Wang, Y.; Yu, W.W. Synthesis of Nitrogen and Sulfur Co-doped Carbon Dots from Garlic for Selective Detection of Fe^{3+}. *Nanoscale Res. Lett.* **2016**, *11*, 1–9. [CrossRef]

139. Chen, J.; Liu, J.; Li, J.; Xu, L.; Qiao, Y. One-pot synthesis of nitrogen and sulfur co-doped carbon dots and its application for sensor and multicolor cellular imaging. *J. Colloid Interface Sci.* **2017**, *485*, 167–174. [CrossRef]

140. Ding, H.; Wei, J.S.; Xiong, H.M. Nitrogen and sulfur co-doped carbon dots with strong blue luminescence. *Nanoscale* **2014**, *6*, 13817–13823. [CrossRef]

141. Liao, S.; Zhao, X.; Zhu, F.; Chen, M.; Wu, Z.; Song, X.; Yang, H.; Chen, X. Novel S, N-doped carbon quantum dot-based "off-on" fluorescent sensor for silver ion and cysteine. *Talanta* **2018**, *180*, 300–308. [CrossRef]

142. Dong, Y.; Pang, H.; Yang, H.B.; Guo, C.; Shao, J.; Chi, Y.; Li, C.M.; Yu, T. Carbon-Based Dots Co-doped with Nitrogen and Sulfur for High Quantum Yield and Excitation-Independent Emission. *Angew. Chem. Int. Ed.* **2013**, *52*, 7800–7804. [CrossRef]

143. Aswathy, B.; Aparna, R.S.; Anjali Devi, J.S.; Sony, G.; Anjana, R.R.; Lekha, G.M.; Praveen, G.L.; Jayasree, M. S,N-doped carbon dots as a fluorescent probe for bilirubin. *Microchim. Acta* **2017**, *185*, 1–11.

144. Zhu, X.; Wang, J.; Zhu, Y.; Jiang, H.; Tan, D.; Xu, Z.; Mei, T.; Li, J.; Xue, L.; Wang, X. Green emitting N,S-co-doped carbon dots for sensitive fluorometric determination of Fe(III) and Ag(I) ions, and as a solvatochromic probe. *Microchim. Acta* **2018**, *185*, 1–10. [CrossRef]

145. Zhou, W.; Zhuang, J.; Li, W.; Hu, C.; Lei, B.; Liu, Y. Towards efficient dual-emissive carbon dots through sulfur and nitrogen co-doped. *J. Mater. Chem. C* **2017**, *5*, 8014–8021. [CrossRef]

146. Bose, M.; Das, N.C.; Ganguly, S.; Mondal, S.; Das, A.K.; Das, P.; Banerjee, S. Heteroatom doped photoluminescent carbon dots for sensitive detection of acetone in human fluids. *Sens. Actuators B Chem.* **2018**, *266*, 583–593.

147. Wei, Z.; Wang, B.; Liu, Y.; Liu, Z.; Zhang, H.; Zhang, S.; Chang, J.; Lu, S. Green synthesis of nitrogen and sulfur co-doped carbon dots from Allium fistulosum for cell imaging. *New J. Chem.* **2019**, *43*, 718–723. [CrossRef]

148. Xu, Y.; Li, D.; Liu, M.; Niu, F.; Liu, J.; Wang, E. Enhanced-quantum yield sulfur/nitrogen co-doped fluorescent carbon nanodots produced from biomass Enteromorpha prolifera: Synthesis, posttreatment, applications and mechanism study. *Sci. Rep.* **2017**, *7*, 1–12. [CrossRef]

149. Zhao, C.; Jiao, Y.; Gao, Z.; Yang, Y.; Li, H. N, S co-doped carbon dots for temperature probe and the detection of tetracycline based on the inner filter effect. *J. Photochem. Photobiol. A Chem.* **2018**, *367*, 137–144. [CrossRef]

150. Xu, S.; Liu, Y.; Yang, H.; Zhao, K.; Li, J.; Deng, A. Fluorescent nitrogen and sulfur co-doped carbon dots from casein and their applications for sensitive detection of Hg^{2+} and biothiols and cellular imaging. *Anal. Chim. Acta* **2017**, *964*, 150–160. [CrossRef]

151. Ye, Q.; Yan, F.; Luo, Y.; Wang, Y.; Zhou, X.; Chen, L. Formation of N, S-codoped fluorescent carbon dots from biomass and their application for the selective detection of mercury and iron ion. *Spectrochim. Acta Part A Mol. Biomol. Spectrosc.* **2017**, *173*, 854–862. [CrossRef]

152. Liu, Y.; Duan, W.; Song, W.; Liu, J.; Ren, C.; Wu, J.; Liu, D.; Chen, H. Red Emission B, N, S-co-Doped Carbon Dots for Colorimetric and Fluorescent Dual Mode Detection of Fe3+ Ions in Complex Biological Fluids and Living Cells. *ACS Appl. Mater. Interfaces* **2017**, *9*, 12663–12672. [CrossRef]

153. Huang, Y.; Cheng, Z. Simple and Green Synthesis of Boron-, Sulfur-, and Nitrogen-Co-Doped Carbon Dots as Fluorescent Probe for Selective and Sensitive Detection of Sunset Yellow. *Nano* **2017**, *12*, 1750123. [CrossRef]

154. Das, R.K.; Mohapatra, S. Highly luminescent, heteroatom-doped carbon quantum dots for ultrasensitive sensing of glucosamine and targeted imaging of liver cancer cells. *J. Mater. Chem. B* **2017**, *5*, 2190–2197. [CrossRef]

155. Yuan, C.; Zhao, Z.; Sun, X.; Hou, L.; Wang, Z.; Zhang, Y.; Chen, Z. Foxtail millet-derived highly fluorescent multi-heteroatoms doped carbon quantum dots towards fluorescent ink and smart nanosensor for selective ion detection. *New J. Chem.* **2018**, *42*, 7326–7331.

156. Khan, W.U.; Wang, D.; Wang, Y. Highly Green Emissive Nitrogen-Doped Carbon Dots with Excellent Thermal Stability for Bioimaging and Solid-State LED. *Inorg. Chem.* **2018**, *57*, 15229–15239. [CrossRef]

157. Hu, C.; Li, M.; Qiu, J.; Sun, Y.-P. Design and fabrication of carbon dots for energy conversion and storage. *Chem. Soc. Rev.* **2019**. [CrossRef]

158. Zhang, Y.-Q.; Ma, D.-K.; Zhang, Y.-G.; Chen, W.; Huang, S.-M. N-doped carbon quantum dots for TiO2-based photocatalysts and dye-sensitized solar cells. *Nano Energy* **2013**, *2*, 545–552. [CrossRef]

159. Wang, H.; Sun, P.; Cong, S.; Wu, J.; Gao, L.; Wang, Y.; Dai, X.; Yi, Q.; Zou, G. Nitrogen-doped carbon dots for "green" quantum dot solar cells. *Nanoscale Res. Lett.* **2016**, *11*, 27. [CrossRef]

160. Mariotti, D.; Padmanaban, D.B.; Rocks, C.; Svrcek, V.; Maguire, P.; Carolan, D. Environmentally friendly nitrogen-doped carbon quantum dots for next generation solar cells. *Sustain. Energy Fuels* **2017**, *1*, 1611–1619.

161. Zhao, Y.; Duan, J.; He, B.; Jiao, Z.; Tang, Q. Improved charge extraction with N-doped carbon quantum dots in dye-sensitized solar cells. *Electrochim. Acta* **2018**, *282*, 255–262. [CrossRef]

162. Yang, Q.; Duan, J.; Yang, W.; Li, X.; Mo, J.; Yang, P.; Tang, Q. Nitrogen-doped carbon quantum dots from biomass via simple one-pot method and exploration of their application. *Appl. Surf. Sci.* **2018**, *434*, 1079–1085. [CrossRef]

163. Wang, Y.; Yan, L.; Ji, G.; Wang, C.; Gu, H.; Luo, Q.; Chen, Q.; Chen, L.; Yang, Y.; Ma, C.-Q.; et al. Synthesis of N,S-Doped Carbon Quantum Dots for Use in Organic Solar Cells as the ZnO Modifier To Eliminate the Light-Soaking Effect. *ACS Appl. Mater. Interfaces* **2019**, *11*, 2243–2253. [CrossRef] [PubMed]

164. Bandi, R.; Devulapalli, N.P.; Dadigala, R.; Gangapuram, B.R.; Guttena, V. Facile Conversion of Toxic Cigarette Butts to N,S-Codoped Carbon Dots and Their Application in Fluorescent Film, Security Ink, Bioimaging, Sensing and Logic Gate Operation. *ACS Omega* **2018**, *3*, 13454–13466. [CrossRef] [PubMed]

165. Liu, Y.; Zhou, L.; Li, Y.; Deng, R.; Zhang, H. Highly fluorescent nitrogen-doped carbon dots with excellent thermal and photo stability applied as invisible ink for loading important information and anti-counterfeiting. *Nanoscale* **2017**, *9*, 491–496. [CrossRef] [PubMed]

166. Fan, C.; Ao, K.; Lv, P.; Dong, J.; Wang, D.; Cai, Y.; Wei, Q.; Xu, Y. Fluorescent Nitrogen-Doped Carbon Dots via Single-Step Synthesis Applied as Fluorescent Probe for the Detection of Fe^{3+} Ions and Anti-Counterfeiting Inks. *Nano* **2018**, *13*, 1850097. [CrossRef]

167. Zhang, R.; Chen, W. Nitrogen-doped carbon quantum dots: Facile synthesis and application as a "turn-off" fluorescent probe for detection of Hg^{2+} ions. *Biosens. Bioelectron.* **2013**, *55*, 83–90. [CrossRef] [PubMed]

168. Huang, H.; Weng, Y.; Zheng, L.; Yao, B.; Weng, W.; Lin, X. Nitrogen-doped carbon quantum dots as fluorescent probe for "off-on" detection of mercury ions, L-cysteine and iodide ions. *J. Colloid Interface Sci.* **2017**, *506*, 373–378. [CrossRef]

169. Huang, H.; Lv, J.-J.; Zhou, D.-L.; Bao, N.; Xu, Y.; Wang, A.-J.; Feng, J.-J. One-pot green synthesis of nitrogen-doped carbon nanoparticles as fluorescent probes for mercury ions. *RSC Adv.* **2013**, *3*, 21691. [CrossRef]

170. Xu, Q.; Li, B.; Ye, Y.; Cai, W.; Li, W.; Yang, C.; Chen, Y.; Xu, M.; Li, N.; Zheng, X.; et al. Synthesis, mechanical investigation, and application of nitrogen and phosphorus co-doped carbon dots with a high photoluminescent quantum yield. *Nano Res.* **2018**, *11*, 3691–3701. [CrossRef]

171. Chandra, S.; Chowdhuri, A.R.; Mahto, T.K.; Laha, D.; Sahu, S.K. Sulphur and nitrogen doped carbon dots: A facile synthetic strategy for multicolour bioimaging, tiopronin sensing, and Hg^{2+} ion detection. *Nano-Struct. Nano-Objects* **2017**, *12*, 10–18. [CrossRef]

172. Wang, Y.; Kim, S.H.; Feng, L. Highly luminescent N, S- Co-doped carbon dots and their direct use as mercury(II) sensor. *Anal. Chim. Acta* **2015**, *890*, 134–142. [CrossRef]

173. Singh, V.K.; Singh, V.; Yadav, P.K.; Chandra, S.; Bano, D.; Kumar, V.; Koch, B.; Talat, M.; Hasan, S.H. Bright-blue-emission nitrogen and phosphorus-doped carbon quantum dots as a promising nanoprobe for detection of Cr(vi) and ascorbic acid in pure aqueous solution and in living cells. *New J. Chem.* **2018**, *42*, 12990–12997. [CrossRef]

174. Erbas-Cakmak, S.; Kolemen, S.; Sedgwick, A.C.; Gunnlaugsson, T.; James, T.D.; Yoon, J.; Akkaya, E.U. Molecular logic gates: The past, present and future. *Chem. Soc. Rev.* **2018**, *47*, 2228–2248. [CrossRef] [PubMed]

175. Liao, S.; Li, X.; Yang, H.; Chen, X. Nitrogen-doped carbon dots rapid and selective detection of mercury ion and biothiol and construction of an IMPLICATION logic gate. *Talanta* **2019**, *194*, 554–562. [CrossRef] [PubMed]

176. Song, J.; Ma, Q.; Zhang, S.; Liu, H.; Guo, Y.; Feng, F. S,N-Co-doped carbon nanoparticles with high quantum yield for metal ion detection, IMP logic gates and bioimaging applications. *New J. Chem.* **2018**, *42*, 20180–20189. [CrossRef]

177. Sharma, V.; Kaur, N.; Tiwari, P.; Saini, A.K.; Mobin, S.M. Multifunctional fluorescent "Off-On-Off" nanosensor for Au3+ and S2− employing N-S co-doped carbon–dots. *Carbon* **2018**, *139*, 393–403. [CrossRef]

178. Wang, W.; Lu, Y.C.; Huang, H.; Wang, A.J.; Chen, J.R.; Feng, J.J. Facile synthesis of N, S-codoped fluorescent carbon nanodots for fluorescent resonance energy transfer recognition of methotrexate with high sensitivity and selectivity. *Biosens. Bioelectron.* **2015**, *64*, 517–522. [CrossRef] [PubMed]

179. Yang, M.; Li, J.; Zhao, Y.; Bian, M.; Hou, C.; Huo, D.; Zou, S. Simple and sensitive fluorescence sensor for methotrexate detection based on the inner filter effect of N, S co-doped carbon quantum dots. *Anal. Chim. Acta* **2018**, *1047*, 179–187.

180. Han, Z.; Zhang, H.; He, L.; Pan, S.; Liu, H.; Hu, X. One-pot hydrothermal synthesis of nitrogen and sulfur co-doped carbon dots and their application for sensitive detection of curcumin and temperature. *Microchem. J.* **2019**, *146*, 300–308. [CrossRef]

181. Wu, B.; Liu, X.; Shi, X.; Han, W.; Wang, C.; Jiang, L. Highly photoluminescent and temperature-sensitive P, N, B-co-doped carbon quantum dots and their highly sensitive recognition for curcumin. *RSC Adv.* **2019**, *9*, 8340–8349. [CrossRef]

182. Li, H.; Sun, C.; Vijayaraghavan, R.; Zhou, F.; Zhang, X.; MacFarlane, D.R. Long lifetime photoluminescence in N, S co-doped carbon quantum dots from an ionic liquid and their applications in ultrasensitive detection of pesticides. *Carbon* **2016**, *104*, 33–39. [CrossRef]

183. Zuo, P.; Liu, J.; Guo, H.; Wang, C.; Liu, H.; Zhang, Z.; Liu, Q. Multifunctional N,S co-doped carbon dots for sensitive probing of temperature, ferric ion, and methotrexate. *Anal. Bioanal. Chem.* **2019**, *411*, 1647–1657. [CrossRef] [PubMed]

184. Shi, W.; Guo, F.; Han, M.; Yuan, S.; Guan, W.; Li, H.; Huang, H.; Liu, Y.; Kang, Z. N,S co-doped carbon dots as a stable bio-imaging probe for detection of intracellular temperature and tetracycline. *J. Mater. Chem. B* **2017**, *5*, 3293–3299. [CrossRef]